# Supporting Information for Publication

# Local and average structure in zinc cyanide: towards an understanding of the atomistic origin of negative thermal expansion

*Simon J. Hibble,*[a] Ann M. Chippindale,*[a] Elena Marelli,[a] Scott Kroeker,*[b] Vladimir K. Michaelis,[b,c] Brandon J. Greer,[b] Pedro M. Aguiar,[d] Edward J. Bilbé,[a] Emma R. Barney,[e,f] and Alex C. Hannon.*[e]*

[a] Department of Chemistry, University of Reading, Whiteknights, Reading, RG6 6AD, UK.

[b] Department of Chemistry, University of Manitoba, Winnipeg, Manitoba, Canada, R3T 2N2.

[c] current address: Department of Chemistry and Francis Bitter Magnet Laboratory, Massachusetts Institute of Technology, Cambridge, Massachusetts 02139 USA.

[d] Department of Chemistry, University of York, York, YO10 5DD, UK.

[e] ISIS Facility, Rutherford Appleton Laboratory, Chilton, Didcot, OX11 0QX, UK.

[f] current address: Faculty of Engineering, University of Nottingham, Nottingham, NG7 2RD UK.

**Contents**

## 1. $^{67}$Zn NMR spectral fitting and peak assignments

Satisfactorily modelling of the $^{67}$Zn NMR spectrum (Figure 4) in terms of the five possible Zn coordination environments present in the $Zn(CN)_{4-n}(NC)_n$ species (Figure 2) requires some knowledge of the respective $C_Q$ values, which cannot be conveniently derived from the highly overlapping set of peaks in Figure 4. We have used theoretical calculations to predict $C_Q$ values for the different Zn environments. Hybrid-DFT calculations on model clusters and GIPAW calculations using periodic boundary conditions (see below) predict a sharp increase in the Zn $C_Q$ values in the $Zn(CN)_{4-n}(NC)_n$ species where $n$ = 1, 2 and 3 in pseudo-tetrahedral geometries (Table 1). Whilst these values cannot be independently measured from the experiments, the calculated $C_Q$ values clearly indicate that the $Zn(CN)_{4-n}(NC)_n$ species where $n$ = 1, 2 and 3, will yield quadrupole-broadened peaks in NMR experiments even at very high applied magnetic fields.

We have used the calculated $C_Q$ values as first estimates to fit the overall composite lineshape, aware that the actual $C_Q$s of the individual species (especially the mixed species) will be only loosely constrained by the experimental fit. Quantum chemical calculations indicate that the $C_Q$s associated with the symmetrical $Zn(CN)_4$ and $Zn(NC)_4$ sites are indeed small and will give rise to narrow NMR peaks at high field. That they are not identically zero, as might be expected from a strictly tetrahedral site, may be attributed to longer-range effects originating from cyanide orientational disorder. Zinc sites with mixed carbon and nitrogen coordination are characterized by much larger $C_Q$ values (>10 MHz), yielding broad NMR peaks. Theoretical quadrupole coupling constants for $Zn(CN)_3(NC)$, $Zn(CN)_2(NC)_2$ and $Zn(CN)(NC)_3$ are comparable in magnitude and the difference in chemical shielding is small relative to the peak widths, resulting in severe signal overlap for these three chemically inequivalent Zn species. The experimental spectrum bears this out, exhibiting few clear features with which to differentiate the mixed-bonding species, but clearly supporting a structural model involving a multiplicity of zinc tetrahedral environments.

Figure 4 shows a best-fit simulation to the experimental spectrum based on computed NMR parameters for each species, where $C_Q$s of 10.5 to 11.5 MHz were obtained for the $Zn(CN)_3(NC)$, $Zn(CN)_2(NC)_2$ and $Zn(CN)(NC)_3$

species and $C_Q$ of 1.2 MHz for the $Zn(CN)_4$ and $Zn(NC)_4$ species. These values are roughly in accord with the calculated values (Table 1), especially considering the documented tendency of CASTEP to overestimate $^{67}$Zn $C_Q$s by 10-15%.[1] Naturally, the fit is not very sensitive to the relative intensities from the three mixed overlapping species, but provides a reliable ratio of 6 : 94 between the combined intensities of the two ordered species (i.e., $Zn(CN)_4$ and $Zn(NC)_4$) and the overall intensities contained in the envelope of the mixed species. The species $Zn(CN)(NC)_3$ and $Zn(CN)_3(NC)$ have essentially axial symmetry along a *pseudo*-$C_{3v}$ axis, which is reflected in the quadrupolar asymmetry parameters of nearly zero. However, $Zn(CN)_2(NC)_2$ possesses lower symmetry and a much larger value of $\eta$, yielding a very different lineshape. Despite the overlap of these three peaks, the $Zn(CN)_2(NC)_2$ signal can be distinguished from the other two by the low-frequency intensity around -1000 ppm. This feature provides additional evidence for the fitted relative intensity of the resonance associated with $Zn(CN)_2(NC)_2$. Hence, even though the $Zn(CN)_3(NC)$ and $Zn(CN)(NC)_3$ signals are indistinguishable in this spectrum, the $Zn(CN)_4$, $Zn(CN)_2(NC)_2$ and $Zn(NC)_4$ signals can be reliably modelled to obtain reasonably accurate peak intensities.

*Assignment of $Zn(CN)_4$ and $Zn(NC)_4$ sites:* Lacking a suitable reference compound, the calculated magnetic shieldings were not converted into $^{67}$Zn chemical shifts for direct comparison with experiment. However, the difference between the two precisely measured chemical shifts ($Zn(CN)_4$ and $Zn(NC)_4$) is 100 ppm (96 ppm, as measured from the MAS spectra, see below). The calculations reproduce this difference reasonably well (143 ppm), with the all-C-bound species, $Zn(CN)_4$, at higher frequency (i.e., lower shielding). Moreover, the differences between shielding parameters for $Zn(CN)_{4-n}(NC)_n$ and $Zn(CN)_{4-(n+1)}(NC)_{(n+1)}$ predicted by GIPAW (Table 1) are in good agreement with those used in fitting the experimental spectrum, despite the large uncertainties in the experimental values for those of the $Zn(CN)_{4-n}(NC)_n$ species, where $n$ = 1, 2 and 3. The shielding differences are 48, 42, 33, 21 ppm (GIPAW calc) compared with 25, 20, 30, 25 (expt).

## 2. Design of Model Clusters for Quantum Chemical Calculations

Hybrid-DFT calculations implemented in Gaussian03[2] used the Becke-3-parameter-Lee-Yang-Parr (B3LYP)[3-6] functional and three different basis sets 6-311++G(d,p)[7-9] (C, N and Zn), aug-cc-pVTZ[10] (Zn only) and aug-cc-pQTZ[11] (Zn only) to reach basis set convergence. Calculations were supported on a SUN X4440 server with 16 cores and 64 GB RAM.

GIPAW calculations were performed using the CASTEP[12] software (Materials Studio 4.4 environment) on an HP xw4400 workstation with a single Intel Dual-Core 2.67 GHz processor and 8 GB DDR RAM. GIPAW-DFT calculations were carried out using periodic boundary conditions on tetrahedral arrays of $Zn(CN)_2$ with all possible local cyanide ordering possibilities. GIPAW calculations were performed using the Perdew-Burke-Ernzerhof (PBE) functional, implementing the generalized gradient approximation (GGA) approach for the exchange-correlation energy.[13,14] Calculations of EFGs[15] and magnetic shielding[16,17] were performed using either coarse or fine accuracy basis set levels, as specified, and a maximum plane-wave energy between 294 and 400 eV. The Monkhorst-Pack grid had a maximum density of up to 4 × 4 × 4 *k*-points.

*Hybrid-DFT.* Clusters of $[Zn_5(CN)_4]^{6+}$ were constructed by alternating carbon and nitrogen ligation to a central zinc to produce all five possible local zinc environments, ranging from $Zn(NC)_4$ (four Zn−N bonds) to $Zn(CN)_4$ (four Zn−C bonds) (Figure 2). Each cyanide was bonded to two Zn atoms to mimic the bridging cyanide configurations found in $Zn(CN)_2$ and the initial structures were geometry-optimized with no symmetry constraints. Reported quadrupolar couplings, $C_Q$, are for the central Zn atom (Table 1).

*GIPAW.* Input files were constructed with starting geometries based on the diffraction data with a modification of the unit cell symmetry (i.e., cubic to triclinic) to accommodate head-to-tail cyanide disorder, where necessary. Five configurations were generated in order to produce the five different combinations of Zn−C and Zn−N bonding arrangements (Figure 2). In addition to single unit cells, four different supercells (2 × 2 × 2 unit cells), each containing 80 atoms, were designed to estimate longer-range geometrical and bonding effects on the zinc quadrupolar coupling constants. For these, the supercell symmetry was primitive and the cyanide orientations were chosen at random to provide roughly equal numbers of each type of Zn species. Both the single unit cell and

supercell models were subjected to an energy minimization procedure to optimize the geometry. The lattice parameter was fixed at 5.92929 Å, typical of several published $Zn(CN)_2$ crystal structures (Table S.3). Average $C_Q$ values from the supercell calculations agree very well with the experimental values used in the best-fit spectral simulation (Table S.1).

The energy-minimized GIPAW calculations on supercells modelling head-to-tail cyanide disorder in $Zn(CN)_2$ provide support for the experimental conclusion from the neutron studies in this paper that the average Zn−N bond length is shorter than the average Zn−C one. A selection of 63 Zn−C and 66 Zn−N bond distances from the supercell calculations, chosen quasi-randomly to include ample representation from all five $Zn(CN)_{4-n}(NC)_n$ species, yielded an average Zn−N bond length of 1.967±0.015 Å and an average Zn−C bond of 1.987±0.014 Å.

**Table S.1**. GIPAW calculations of $^{67}$Zn $C_Q$ values in supercell (2 × 2 × 2) models of $Zn(CN)_2$ with quasi-random cyanide orientations. The average $C_Q$ values are reported for *N* examples of each type of Zn site in the geometry-optimized supercell calculations.

| *Zn fragment* | *N* | *Average* $C_Q$ / MHz |
|---|---|---|
| $Zn(CN)_4$ | 10 | 2.9 ± 1.3 |
| $Zn(CN)_3(NC)$ | 13 | 11.3 ± 2.0 |
| $Zn(CN)_2(NC)_2$ | 16 | 11.8 ± 1.4 |
| $Zn(CN)(NC)_3$ | 17 | 10.8 ± 1.4 |
| $Zn(NC)_4$ | 8 | 2.7 ± 1.3 |

## 3. Calculation of $^{67}$Zn NMR excitation efficiencies in $Zn(CN)_2$

In principle, the excitation efficiency for $^{67}$Zn might be expected to have some dependence on $C_Q$ and hence vary for the different Zn species in $Zn(CN)_2$. This would have the result that the measured signal intensities would not accurately represent the actual site populations in the sample. Since there is a large difference between the $C_Q$ values for the $Zn(CN)_{4-n}(NC)_n$ species, we have calculated the relative excitation efficiencies for the five Zn

species in Figure 2. The numerical calculation of excitation efficiencies is straightforward using programs such as SIMPSON,[18] but usually requires a fairly precise knowledge of the $C_Q$ values, especially when $C_Q$s are small. In the present case, the excitation efficiencies of the large-$C_Q$ species (10-12 MHz) are found to be insensitive to deviations of ±1 MHz or larger, whereas the efficiencies of small-$C_Q$ species (i.e., < 1 MHz) are much more sensitive to their magnitudes. Therefore, every effort has been made to constrain the $C_Q$ values for a suitable assessment of excitation efficiencies by SIMPSON. The resulting correction factors alter the directly measured intensities by less than 5% (relative), well within the measurement uncertainty and therefore the original values are retained for the purpose of this discussion.

The calculation of excitation efficiencies for quadrupolar nuclei requires a reasonably accurate assessment of $C_Q$ values. The increasing reliability of high-level theoretical calculations makes it tempting to simply accept these values as correct in the absence of precise experimental quantities. However, the presence of longer-range effects in a disordered structure influence the EFG, even for the $Zn(CN)_4$ and $Zn(NC)_4$ species. Hence, the accuracy of the parameters predicted from the cluster models will be compromised by truncation errors, whereas the periodic calculations will be biased by the non-physical imposition of repeating unit cells. Despite these caveats, the agreement between the two computational approaches is remarkable (Table 1). Where it breaks down is for the $Zn(CN)_4$ and $Zn(NC)_4$ species, with the GIPAW single-cell calculations predicting perfectly cubic Zn environments (i.e., no electric field gradient), an artifact of the order artifically imposed by periodic boundary conditions. To evaluate qualitatively the extent of longer-range effects on the $C_Q$s of the symmetrical sites, we ran a series of GIPAW calculations on four 2 × 2 × 2 supercells (i.e., 16 Zn atoms) with selected cyanide ligands inverted to mimic the disorder present in $Zn(CN)_2$. This introduces distortions in the local symmetry and geometry at Zn such that $C_Q$ values for the $Zn(CN)_4$ and $Zn(NC)_4$ species increase significantly, confirming that the longer-range structural effects associated with disorder have a non-negligible influence on the NMR parameters by virtue of electronic and geometrical distortions. These data are summarized in Table S.1, where it can be seen that the average $C_Q$s increase significantly with respect to the single unit-cell calculations (e.g., from zero to > 2 MHz). Considering the limitations inherent in this modelling approach and the large range of calculated values, these

cannot be accepted as reliable numerical predictions but serve to confirm the importance of long-range structural effects on reducing the symmetry at Zn and increasing the $C_Q$s.

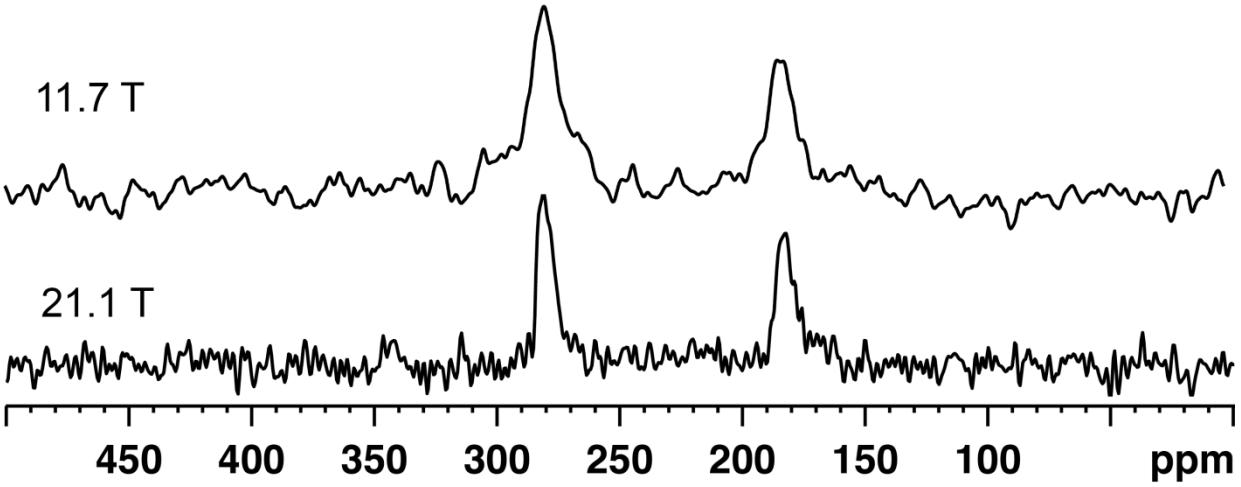


**Figure S.1.** $^{67}$Zn rotor-synchronized Hahn-echo MAS NMR spectrum of $Zn(CN)_2$ recorded at 11.7 T (4 mm probe; spinning rate: 14 kHz; recycle delay: 0.5 s; number of transients: 512k) and 21.1 T (7 mm probe; spinning rate: 3.5 kHz; recycle delay: 5 s; number of transients: 12800). Under these conditions, only the narrow signals arising from $Zn(CN)_4$ and $Zn(NC)_4$ are observed.

We compared the experimentally determined $^{67}$Zn magic-angle spinning (MAS) NMR linewidths of the symmetrical species, $Zn(CN)_4$ and $Zn(NC)_4$, at two fields, 11.7 and 21.1 T, to assess the extent of second-order quadrupolar broadening (Figure S.1). To our surprise, the linewidths are almost identical at 11.7 and 21.1 T, implying that the peaks are not uniformly dominated by second-order quadrupolar broadening. The peak at 184 (181) ppm is 540±20 (590±50) Hz, and the peak at 281 (276) ppm is 460±20 (500±40) Hz for the 21.1 (11.7) T data set. If second-order quadrupolar broadening were solely responsible for the observed peak widths, the low-field data would place an upper bound on the $C_Q$ of 1.2 MHz. However, the lack of peak narrowing at higher field implies that other broadening effects are involved. One source of broadening is the combined effect of indirect spin-spin coupling and residual dipolar coupling to the directly bonded $^{14}$N nuclei.[19,20] Whilst the effect of such coupling normally introduces asymmetric peak shapes, the structural disorder in the present case obscures any

obvious asymmetry. Based on comparisons of reduced coupling constants in tetrahedral metal cyanides,[21,22] $^{1}J(^{67}Zn,^{14}N)$ is estimated to be 20-30 Hz, which would account for broadening of up to 250 Hz for the $Zn(NC)_4$ site. Indeed, the lower-frequency peaks in spectra at both fields are slightly broader than the higher-frequency peaks, leading to support for the assignment of the former to $Zn(NC)_4$, since no such residual dipolar coupling would be present for $Zn(CN)_4$. This assignment is supported by GIPAW calculations, where the N−bound Zn shieldings are greater than those of C−bound Zn (Table 1), leading to progressively lower chemical shifts with successive replacement of C by N ligation. The fact that there is such a subtle difference between the two peak widths at a given field implies that other broadening effects are prominent. Because of the structural disorder in this system, longer-range environmental effects will cause distributions in both $C_Q$ and chemical shift. Since second-order quadrupolar broadening will be significantly reduced at high field while the chemical shift distribution will be accentuated, the observed peak width at 21.1 T is likely dominated by the latter. Under the assumption that second-order quadrupolar broadening dominates the 11.7 T MAS peak widths whereas chemical shift distribution dominates the 21.1 T MAS peak widths, we estimate the average $C_Q$ of the symmetrical sites to be 1.2 ± 0.25 MHz. Close inspection of the $^{67}$Zn NMR spectrum of Figure 4 reveals the hint of some signal intensity around +1300 and -1200 ppm, which would correspond to the "horns" of the inner satellite transitions for an axially symmetric ($\eta$ = 0) Zn site with $C_Q$ = 1.05 MHz. Although their low intensity precludes positive identification, their positions would support our $C_Q$ estimates. Other approaches to evaluating $C_Q$s include observing the spinning sideband intensities as a measure of the full extent of the satellite transition manifold and measuring the nutation behavior of the individual peaks. However, the inherently low sensitivity of $^{67}$Zn makes both approaches impracticable.

Nutation simulations were carried out using SIMPSON 3.1.0[18] on an Apple MacBook Pro (2.3 GHz Intel Core i5) using conditions identical to those employed experimentally. Only single-quantum coherences were retained after the initial pulse and detection was carried out on the central transition. Simulations were averaged over 28656 orientations using the zcw scheme to ensure suitable averaging for the even the largest $C_Q$ sites. Pulse bandwidth and/or offset effects were accounted for by ensuring that simulations retained the experimental peak positions with respect to the transmitter. Additional simulations were performed with detection of all coherences for two sites (at

the extremes of the $C_Q$ range) to verify that satellite transitions make no significant contribution to the observed signal under the experimental conditions.

With the $C_Q$ values determined above, SIMPSON calculations of our solid-echo non-spinning $^{67}$Zn NMR experiments yield the correction factors listed in Table S.2 with which to convert integrated peak intensities into zinc site populations. Fortuitously, the correction factors prove to be very similar and have no significant effect on the measured values.

**Table S.2.** Intensity correction factors calculated by SIMPSON[18] using our best estimates of the average $C_Q$ values.

| | $\delta_{iso}$ / ppm | $C_Q$ /MHz | $\eta$ | $I_{expt}$ / % | *Correction Factor*[*] | *Corrected Populations* / %[‡] |
|---|---|---|---|---|---|---|
| $Zn(CN)_4$ | 275 | 1.2 ± 0.2 | 0.0 | 3.5 | 0.720 (0.755, 0.712) | 3.35 |
| $Zn(NC)(CN)_3$ | 250 | 11.0 ± 1.0 | 0.0 | 15 | 0.708 (0.716, 0.696) | 14.59 |
| $Zn(NC)_2(CN)_2$ | 220 | 11.5 ± 1.0 | 0.85 | 64 | 0.678 (0.697, 0.653) | 65.0 |
| $Zn(NC)_3(CN)$ | 200 | 10.5 ± 1.0 | 0.0 | 15 | 0.703 (0.713, 0.688) | 14.69 |
| $Zn(NC)_4$ | 175 | 1.2 ± 0.2 | 0.0 | 2.5 | 0.727 (0.762, 0.720) | 2.37 |

[*]Corrections factors and their maximum and minimum values (in parentheses) are calculated from the best estimated $C_Q$ values and their standard deviations, respectively. [‡]The corrected populations are obtained by dividing the experimental intensities, $I_{expt}$, by the corresponding correction factors and normalizing to 100%.

## 4. Variation of Lattice Parameter and C≡N Bond Length with Temperature

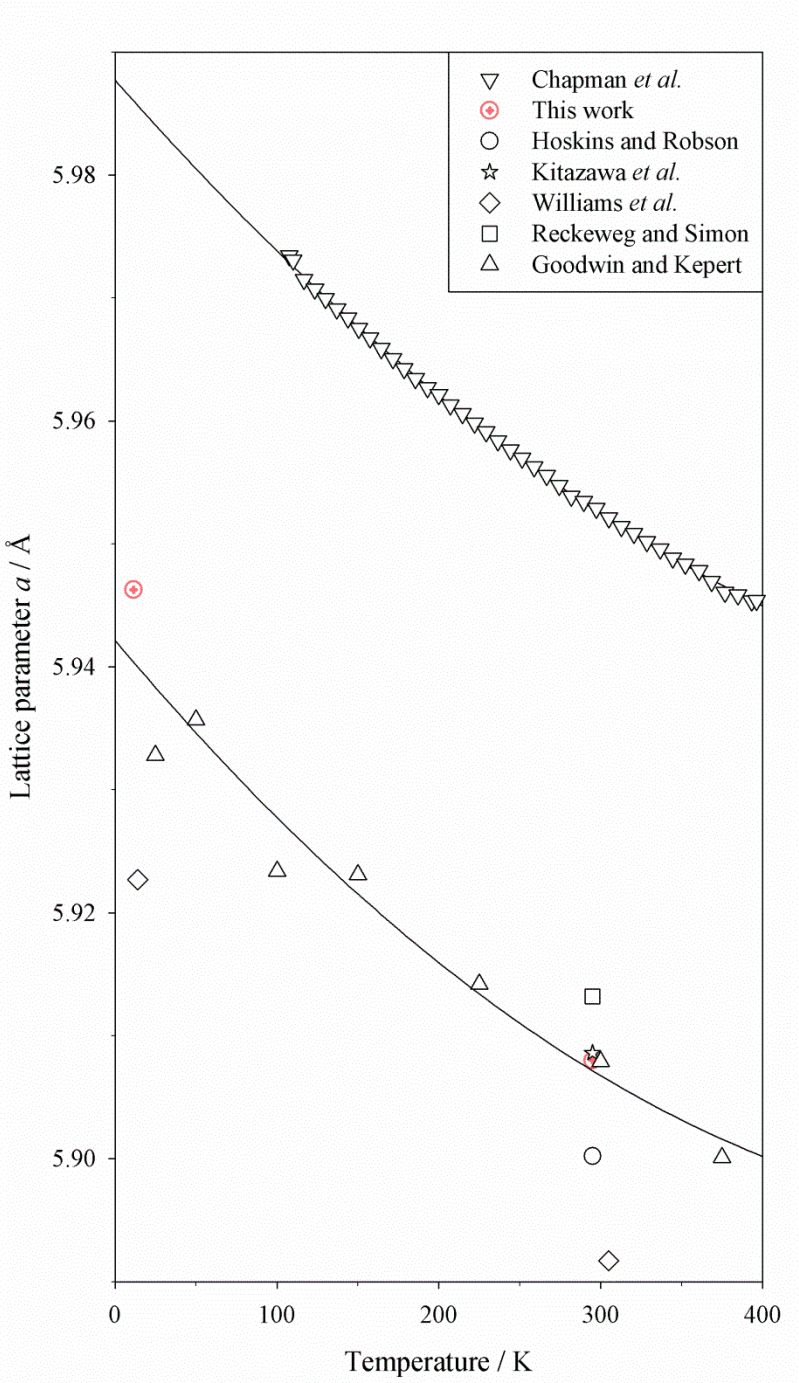


**Figure S.2.** The temperature-dependence of the lattice parameter, *a*, of $Zn(CN)_2$. The symbols correspond to those given in Table S.3. The upper line is a quadratic fit to the results of Chapman et al.,[23] whilst the lower line is a quadratic fit to the current results together with those of Goodwin and Kepert.[24] For other references, see Table S.3.

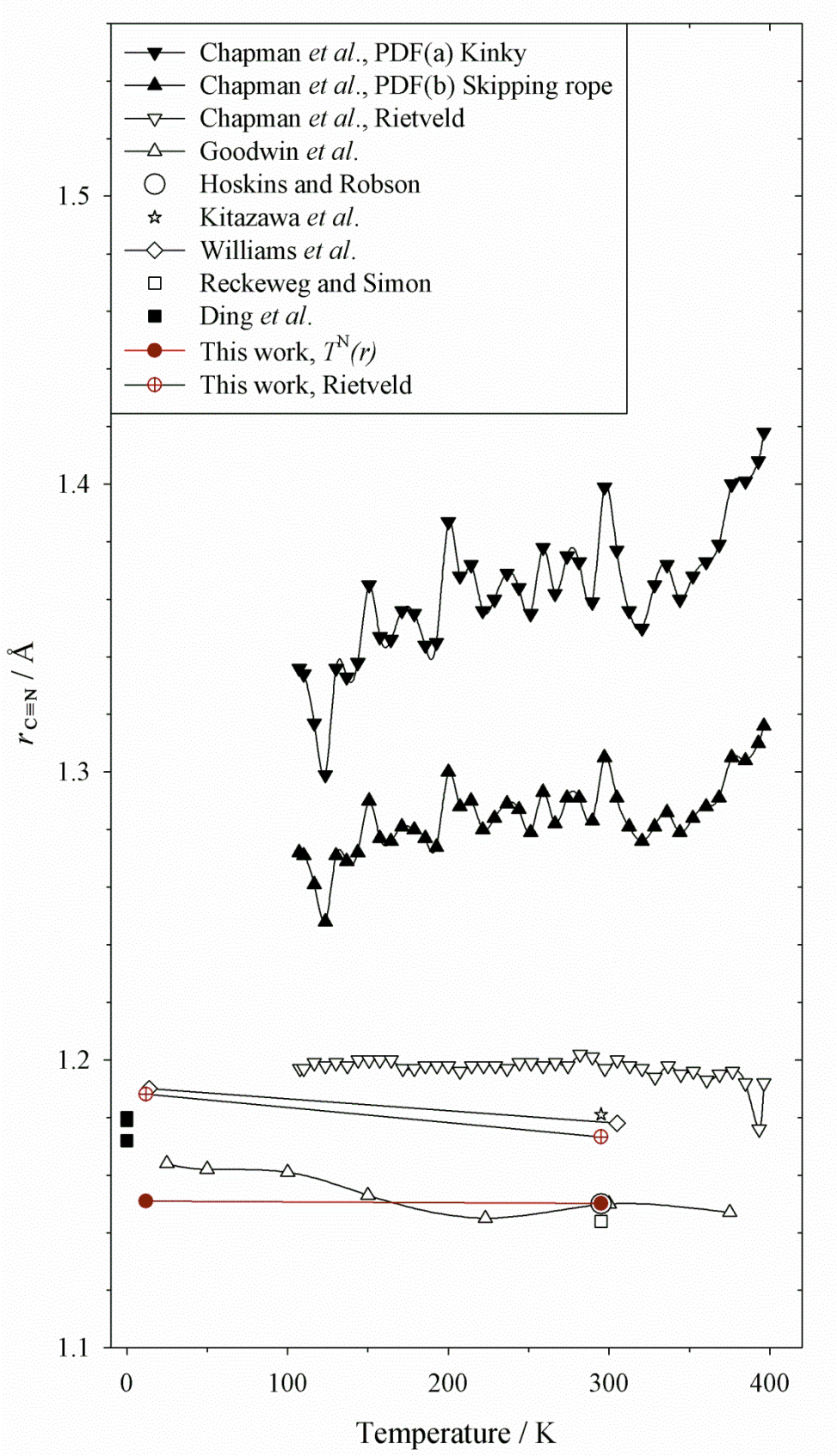


**Figure S.3.** The temperature-dependence of the C≡N bond length in $Zn(CN)_2$. The symbols and references correspond to those given in Table S.3.

**Table S.3.** The temperature-dependence of the lattice parameter and bond lengths in $Zn(CN)_2$.

| Source | Symbol in Figure S.3 | Method | Temperature / K | *a* / Å | $r_{C\equiv N}$ /Å | $r_{Zn-C/N}$ /Å | |
|---|---|---|---|---|---|---|---|
| Zhdanov[25] | | XRD | 295 | 5.9 | 1.022 | 2.044 | |
| Hoskins and Robson[26] | ○ | single crystal XRD | 295 | 5.9002(9) | 1.150(5) | Zn–N = 2.037(5) | Zn–C = 1.923(6) |
| Kitazawa et al.[27] | ☆ | single crystal XRD | 295 | 5.9086(7) | 1.181 | 1.968 | |
| Williams et al. [28] | M | ND Rietveld | 14 | 5.9227(1) | 1.190 | 1.970 | |
| | | | 305 | 5.8917(1) | 1.178 | 1.962 | |
| Reckeweg and Simon[29] | □ | single crystal XRD | 295 | 5.9132(7) | 1.144 | 1.988 | |
| Goodwin and Kepert[24] | △ | single crystal XRD | 25 | 5.9328(3) | 1.164 | 1.987 | |
| | | | 300 | 5.9079(1) | 1.150 | 1.989 | |
| Chapman et al.[23] | ▼ | XRD PDF | 107.3 | | *1.336* [a] | 2.0149(8) | |
| | | | 297.1 | | *1.399* [a] | 2.0187(10) | |
| Chapman et al.[23] | ▲ | XRD PDF | 107.3 | | *1.272* [b] | 2.0149(8) | |
| | | | 297.1 | | *1.305* [b] | 2.0187(10) | |
| Chapman et al.[23] | ▽ | XRD Rietveld | 107.6 | 5.97342(1) | 1.197(4) | 1.988(3) | |
| | | | 297.4 | 5.95290(2) | 1.197(5) | 1.979(3) | |
| This work | ⊕ | ND Rietveld | 11.4 | 5.9463(6) | 1.1881(7) | 1.9808(4) | |
| | | | 295 | 5.908(3) | 1.173(2) | 1.972(1) | |
| | ● | ND PDF | 11.4 | - | 1.1510(2) | 1.9914(5) | |
| | | | 295 | - | 1.1502(3) | 1.9955(6) | |

In a number of papers, the authors report the lattice parameter at a number of temperatures. In these cases, only the two values at temperatures closest to those used in this work are quoted.

The $r_{C\equiv N}$ values of Chapman et al.[23] denoted *a* and *b*, are derived values corresponding to the *kinky* and *skipping-rope* models, respectively

## 5. Neutron Diffraction Measurements on $Zn(CN)_2$

Time-of-flight (TOF) neutron diffraction was performed on the GEM diffractometer[30] at the ISIS Facility, Rutherford Appleton Laboratory, Chilton, Didcot, UK. The absolute calibration[31] of $Lsin\theta$ (where $L$ is the total flight path and $2\theta$ is the scattering angle) for each detector was achieved using diffraction data measured on crystalline $Y_3Al_5O_{12}$. For the treatment of data for Rietveld analysis, the values of $Lsin\theta$ were refined so as to yield the reported lattice parameter of this compound.[32] For the treatment of data for total diffraction analysis, the values of $Lsin\theta$ were refined to ensure that a number of well-defined peaks in the correlation function occur at the correct interatomic distances. For this refinement, only correlation function peaks whose positions depend solely on the lattice parameter were used i.e., the correlations involve only atoms on special positions where all coordinates $x$, $y$ and $z$ are fixed. The uncertainty in the absolute values of the interatomic distances arising from the total diffraction calibration is approximately 0.1%. The small difference (~0.27%) between the two calibrations described here is due to the asymmetric peak shape for TOF neutron diffraction.[33]

For the neutron diffraction measurements, 2.9221 g of $Zn(CN)_2$ were sealed inside a vanadium can of inner and outer diameters of 0.381 and 0.394 cm, respectively. The packing density of the sample, used to evaluate the corrections for attenuation and multiple scattering, was determined from the sample mass and volume. The diffraction pattern was measured at 295 K and then, by placing the sample inside a closed cycle refrigerator (CCR), at 11.4 K. Background runs were collected on the empty can, CCR and diffractometer, and data for absolute normalization were collected for a standard vanadium rod of diameter 0.834 cm. The programs GudrunN[34] and ATLAS[35] were used to correct the data for multiple scattering, attenuation and inelasticity, and to normalize to absolute cross-section units. Applying the same data reduction and correction procedures for the data before Rietveld and total diffraction analyses ensures that the results from the two approaches are strictly compatible. A particular advantage of carrying out the rigorous data correction procedure above, which is not normally applied before Rietveld analysis, is that the resultant atomic displacement parameters will be of high reliability.

## 6. Rietveld Analysis of Neutron Diffraction Data using GSAS[36,37]

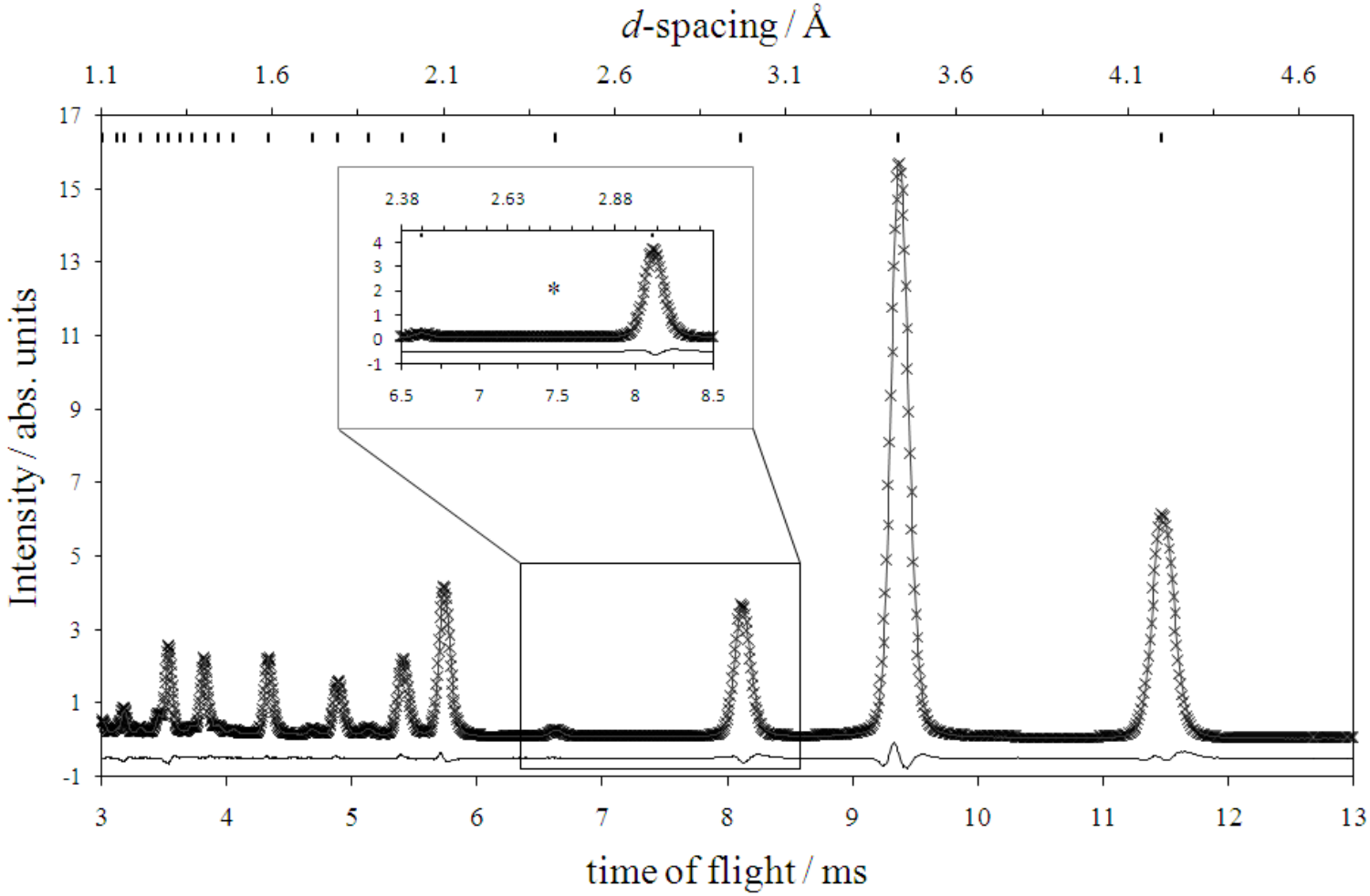


**Figure S.4.** Powder neutron diffraction profile fit for Bank 3 data (GEM diffractometer) of $Zn(CN)_2$ at 11.4 K in space group $Pn\bar{3}m$. Experimental data are shown as crosses and the fit is shown as a black line. The difference between the experimental data and fit is shown at the bottom of the graph and the calculated peak positions are shown as vertical lines at the top of the graph. The asterisk indicates the position of a peak which would be observed if the structure were ordered i.e., in space group $P\bar{4}3m$.

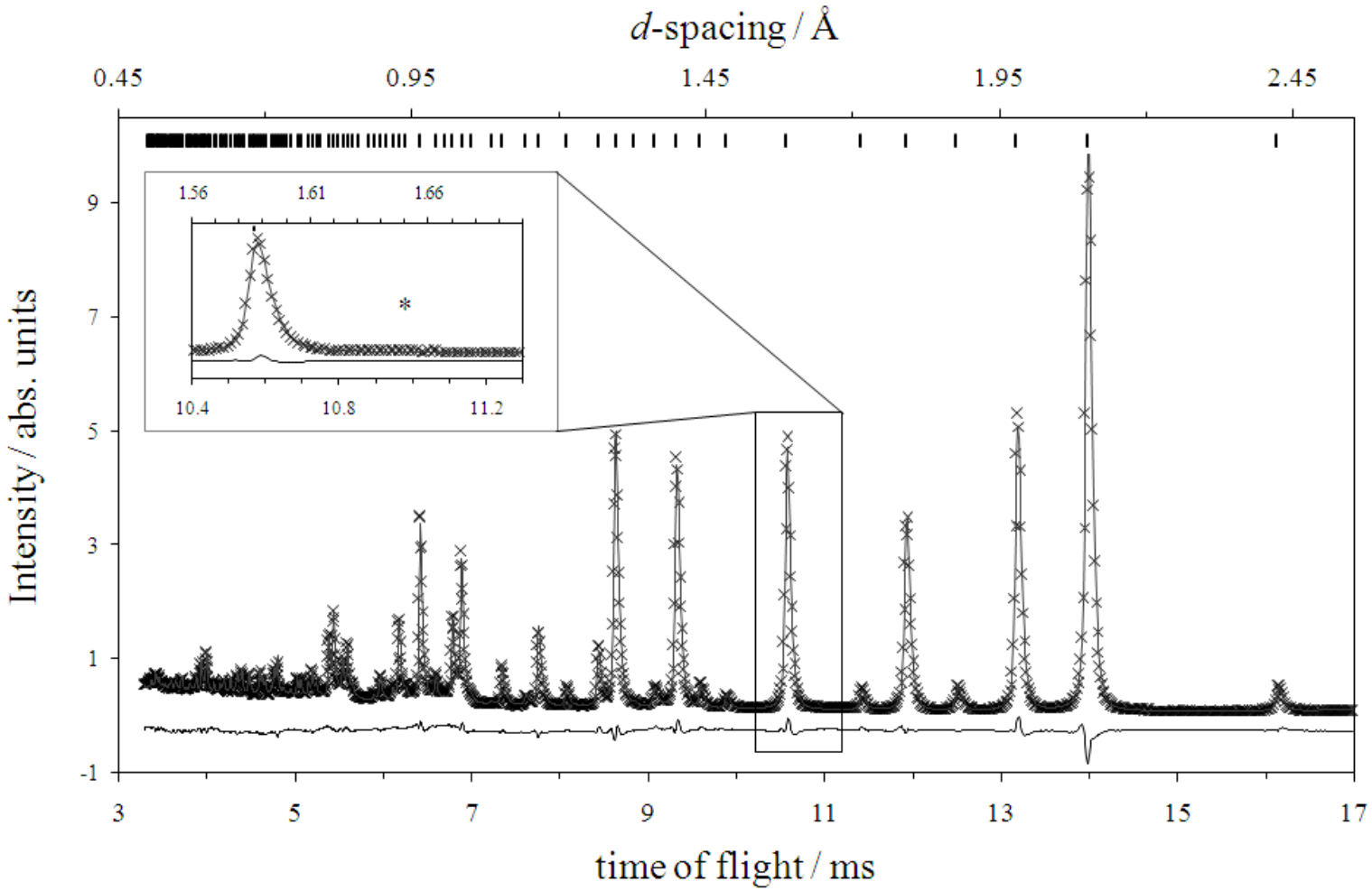


**Figure S.5**. Powder neutron diffraction profile fit for Bank 5 data (GEM diffractometer) of $Zn(CN)_2$ at 11.4 K in space group $Pn\bar{3}m$. Experimental data are shown as crosses and the fit is shown as a black line. The difference between the experimental data and fit is shown at the bottom of the graph and the calculated peak positions are shown as vertical lines at the top of the graph. The asterisk indicates the position of a peak which would be observed if the structure were ordered i.e., in space group $P\bar{4}3m$.

**Table S.4.** Crystallographic Details and Rietveld Parameters for $Zn(CN)_2$ at 11.4 and 295 K.

| | 11.4 K | | | 295 K | | |
|---|---|---|---|---|---|---|
| Space group | $Pn\bar{3}m$ | | $P\bar{4}3m$ | $Pn\bar{3}m$ | | $P\bar{4}3m$ |
| $Z$ | 2 | | 2 | 2 | | 2 |
| Detector Bank 3 *t-o-f* range / ms | 3.005 – 13.000 | | 3.005 – 13.000 | 3.064 – 13.000 | | 3.064 – 13.000 |
| Detector Bank 5 *t-o-f* range / ms | 3.300 – 17.000 | | 3.300 – 17.000 | 3.135 – 17.000 | | 3.135 – 17.000 |
| $N_{data}$, $N_{obs}$ for Banks (3 +5) | 3235, 260 | | 3235, 260 | 3268, 268 | | 3268, 268 |
| *refinement type* | isotropic | anisotropic | isotropic[§] | isotropic | anisotropic | isotropic[§] |
| $a$ / Å | 5.9463(6) | 5.9464(6) | 5.9463(7) | 5.908(3) | 5.908(3) | 5.907(3) |
| $V$ / Å$^3$ | 210.25(7) | 210.26(7) | 210.25(8) | 206.2(3) | 206.25(7) | 206.3(3) |
| $\rho_{calc}$ / g cm$^{-3}$ | 1.855 | 1.855 | 1.855 | 1.891 | 1.891 | 1.891 |
| $N_{par}$[‡] | 28 | 29 | 31 | 28 | 29 | 31 |
| $R_p$ , $wR_p$ Banks (3 +5) / % | 4.25, 5.48 | 4.26, 5.40 | 4.84, 6.08 | 5.44, 8.83 | 5.27, 8.29 | 5.89, 9.73 |
| *fractional coordinates* | Table S.5 | Table S.6 | Table S.7 | Table S.8 | Table S.9 | Table S.10 |

[§] refinements of the anisotropic displacement parameters using space group $P\ 3m$ produce physically meaningless values

[‡] The 28 parameters included in isotropic refinements using space group $Pn\ m$ are: lattice parameter $a$; $U_{iso}$ for Zn; $x$ and $U_{iso}$ for C/N;
and for Bank 3 data: scale factor, 6 background parameters, 5 profile parameters ($\sigma_1$, $\sigma_2$, $\gamma_1$, zero and absorption); and for Bank 5 data: scale factor, 6 background parameters, 5 profile parameters ($\sigma_1$, $\sigma_2$, $\gamma_1$, zero and absorption).

The 31 parameters included in isotropic refinements using space group $P\ 3m$ are: the $a$ lattice parameter; $U_{iso}$ for Zn(1) and for Zn(2); $x$ and $U_{iso}$ for C and N; for Bank 3 data: scale factor, 6 background parameters, 5 profile parameters ($\sigma_1$, $\sigma_2$, $\gamma_1$, zero and absorption); and for Bank 5 data: scale factor, 6 background parameters, 5 profile parameters ($\sigma_1$, $\sigma_2$, $\gamma_1$, zero and absorption).

**Table S.5.** Fractional atomic coordinates and displacement parameters for $Zn(CN)_2$ ($Pn\bar{3}m$) at 11.4 K (isotropic refinement).

| | Site | *x* | *y* | *z* | Occ | $U_{iso}$ / Å$^2$ |
|---|---|---|---|---|---|---|
| Zn | 2*a* | 0 | 0 | 0 | 1 | 0.0097(3) |
| C/N | 8*e* | 0.19232(4) | 0.19232(4) | 0.19232(4) | 0.5/0.5 | 0.0115(1) |

**Table S.6.** Fractional atomic coordinates and displacement parameters for $Zn(CN)_2$ ($Pn\bar{3}m$) at 11.4 K (anisotropic refinement).

| | Site | *x* | *y* | *z* | Occ | $U_{ii}$ / Å$^2$ | $U_{ij}$ / Å$^2$ |
|---|---|---|---|---|---|---|---|
| Zn | *2a* | 0 | 0 | 0 | 1 | 0.0095(3) | 0 |
| C/N | *8e* | 0.19238(4) | 0.19238(4) | 0.19238(4) | 0.5/0.5 | 0.0117(1) | -0.0014(1) |

**Table S.7.** Fractional atomic coordinates and displacement parameters for $Zn(CN)_2$ ($P\bar{4}3m$) at 11.4 K (isotropic refinement).

| | Site | *x* | *y* | *z* | Occ | $U_{iso}$/ Å$^2$ |
|---|---|---|---|---|---|---|
| Zn(1) | *1a* | 0 | 0 | 0 | 1 | 0.008(1) |
| Zn(2) | *1b* | 1/2 | 1/2 | 1/2 | 1 | 0.012(2) |
| C | *4e* | 0.1915(3) | 0.1915(3) | 0.1915(3) | 1 | 0.0037(4) |
| N | *4e* | 0.3068(2) | 0.3068(2) | 0.3068(2) | 1 | 0.0186(5) |

**Table S.8.** Fractional atomic coordinates and displacement parameters for $Zn(CN)_2$ ($Pn\bar{3}m$) at 295 K (isotropic refinement).

| | Site | *x* | *y* | *z* | Occ | $U_{iso}$ / Å$^2$ |
|---|---|---|---|---|---|---|
| Zn | 2*a* | 0 | 0 | 0 | 1 | 0.036(1) |
| C/N | *8e* | 0.19267(9) | 0.19267(9) | 0.19267(9) | 0.5/0.5 | 0.0436(6) |

**Table S.9.** Fractional atomic coordinates and displacement parameters for $Zn(CN)_2$ ($Pn\bar{3}m$) at 295 K (anisotropic refinement).

| | Site | *x* | *y* | *z* | Occ | $U_{ii}$ / Å$^2$ | $U_{ij}$ / Å$^2$ |
|---|---|---|---|---|---|---|---|
| Zn | *2a* | 0 | 0 | 0 | 1 | 0.036(1) | 0 |
| C/N | *8e* | 0.19289(8) | 0.19289(8) | 0.19289(8) | 0.5/0.5 | 0.0463(6) | -0.0114(5) |

**Table S.10.** Fractional atomic coordinates and displacement parameters for $Zn(CN)_2$ ($P\bar{4}3m$) at 295 K (isotropic refinement).

| | Site | *x* | *y* | *z* | Occ | $U_{iso}$/ Å$^2$ |
|---|---|---|---|---|---|---|
| Zn(1) | *1a* | 0 | 0 | 0 | 1 | 0.019(6) |
| Zn(2) | *1b* | 1/2 | 1/2 | 1/2 | 1 | 0.058(6) |
| C | *4e* | 0.1887(4) | 0.1887(4) | 0.1887(4) | 1 | 0.0245(8) |
| N | *4e* | 0.3030(5) | 0.3030(5) | 0.3030(5) | 1 | 0.077(2) |

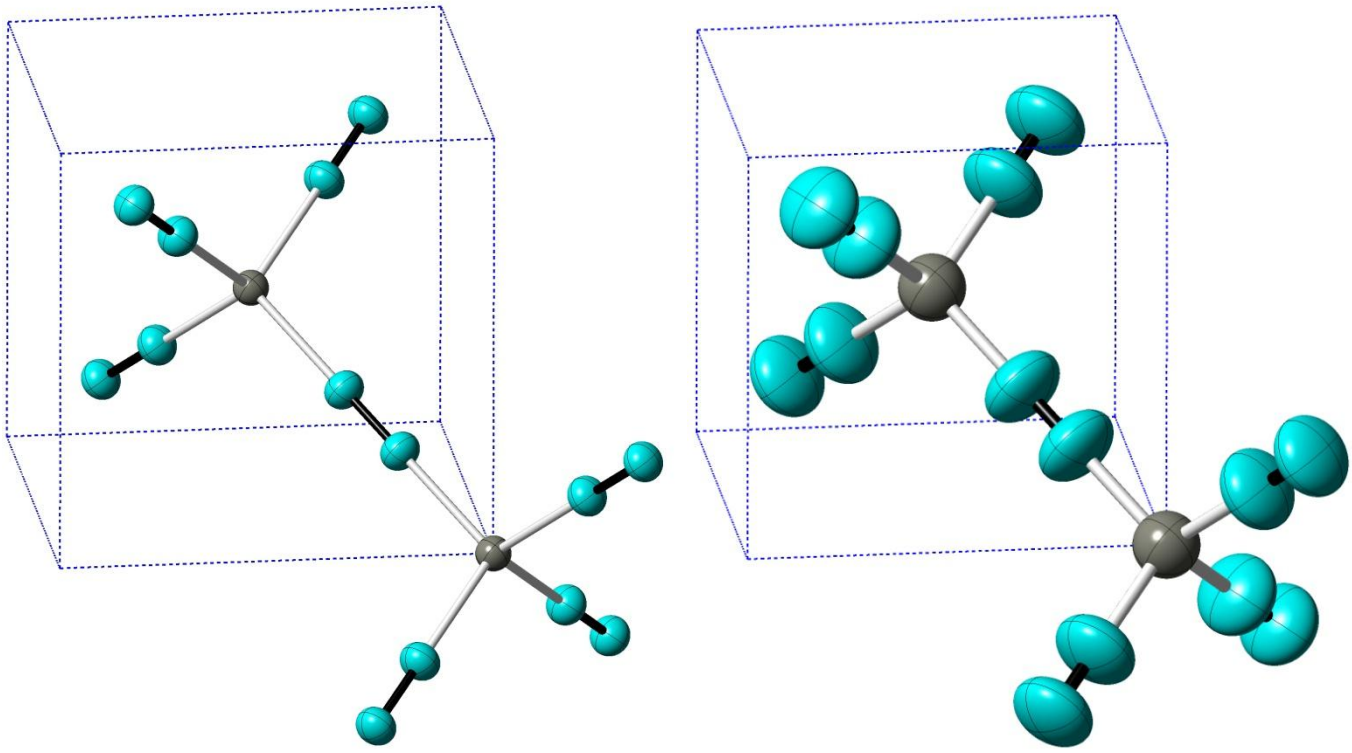

**Figure S.6.** The anisotropic displacement ellipsoids (90% probability) at 11.4 K (left) and at 295 K (right) calculated from data in Tables S.6 and S.9 (space group $Pn\bar{3}m$).

**Table S.11.** Interatomic distances in the average structure of $Zn(CN)_2$ at 11.4 K, derived from the results of Rietveld analysis of the neutron diffraction data from Table S.6 (using the notation shown in Figures 6 and S.7 for the intra- and inter-network distances, respectively).

| | Interatomic distance, $r_{p–q}$ /Å | Atom pair, $p$–$q$ | Coordination number, $n_{p–q}$ | Intra-network or inter-network |
|---|---|---|---|---|
| $r_1$ | 1.187 | C≡N | 1 | intra |
| $r_2$ | 1.981 | Zn–C/N | 4 | intra |
| $r_3$ | 3.168 | Zn···C/N | 4 | intra |
| $r_4$ | 3.236 | (C/N)···(C/N) | 3 | intra |
| $r_5$ | 4.260 | (C/N)···(C/N) | 6 | intra |
| $r_6$ | 4.260 | (C/N)···(C/N) | 6 | inter |
| $r_7$ | 4.315 | (C/N)···(C/N) | 6 | inter |
| $r_8$ | 4.862 | Zn···C/N | 12 | inter |
| $r_9$ | 5.068 | Zn···C/N | 12 | inter |
| $r_{10}$ | 5.150 | Zn···Zn | 4 | intra |
| $r_{11}$ | 5.150 | Zn···Zn | 4 | inter |
| $r_{12}$ | 5.174 | (C/N)···(C/N) | 3 | intra |
| $r_{13}$ | 5.350 | (C/N)···(C/N) | 3 | inter |

Note: The shortest internetwork distance in $Zn(CN)_2$ occurs at 4.260 Å.

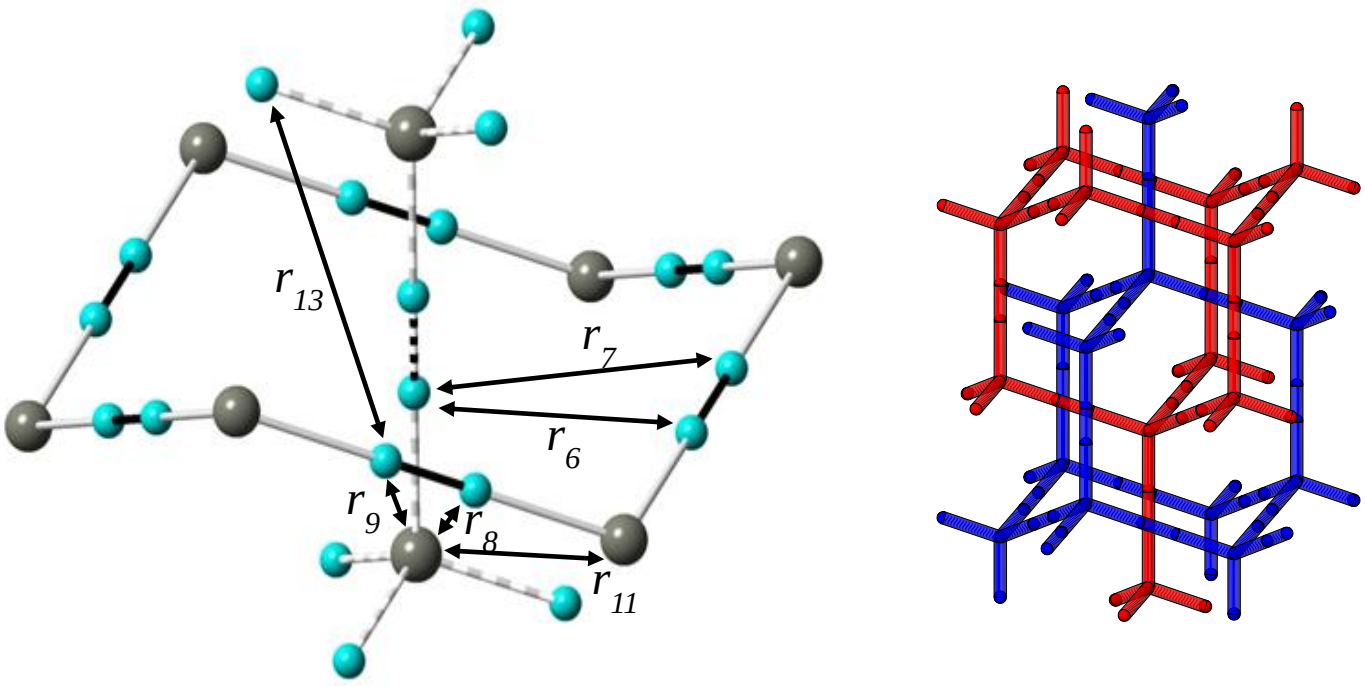


**Figure S.7.** Structure of $Zn(CN)_2$, showing (left) interatomic distances between atoms in the two networks. (Intranetwork distances are shown in Figure 6) and (right) the two interpenetrating networks (red and blue).

**Table S.12.** Displacement tensors and Eigenvalues calculated from the Anisotropic displacement parameters given in Tables S.6 and S.9 (space group, $Pn\bar{3}m$ ).

| | 11.4 K | 295 K |
|---|---|---|
| Displacement tensor for C/N, $U_{ij}$/ Å$^2$ | $\begin{pmatrix} 0.0117 & -0.0014 & -0.0014 \\ -0.0014 & 0.0117 & -0.0014 \\ -0.0014 & -0.0014 & 0.0117 \end{pmatrix}$ | $\begin{pmatrix} 0.0463 & -0.0114 & -0.0114 \\ -0.0114 & 0.0463 & -0.0114 \\ -0.0114 & -0.0114 & 0.0463 \end{pmatrix}$ |
| Principal components (Eigenvalues of the displacement tensor, $U_{ij}$) for C/N / Å$^2$ | $\begin{pmatrix} 0.013 \\ 0.013 \\ 0.0094 \end{pmatrix}$ | $\begin{pmatrix} 0.058 \\ 0.058 \\ 0.024 \end{pmatrix}$ |
| Mean square displacement of C/N perpendicular to the Zn···Zn axis, $U_{\perp}$ / Å$^2$ | 0.013 | 0.058 |
| Mean square displacement of C/N parallel to the Zn···Zn axis , $U_{\parallel}$ / Å$^2$ | 0.0094 | 0.024 |
| Mean displacement of C/N perpendicular to the Zn···Zn axis, $u_{\perp}$ / Å | 0.114 | 0.241 |
| Mean displacement of C/N parallel to the Zn···Zn axis , $u_{\parallel}$ / Å | 0.097 | 0.152 |
| Displacement tensor for Zn, $U_{ij}$/ Å$^2$ | $\begin{pmatrix} 0.0095 & 0 & 0 \\ 0 & 0.0095 & 0 \\ 0 & 0 & 0.0095 \end{pmatrix}$ | $\begin{pmatrix} 0.036 & 0 & 0 \\ 0 & 0.036 & 0 \\ 0 & 0 & 0.036 \end{pmatrix}$ |
| Principal components (Eigenvalues of the displacement tensor, $U_{ij}$) for Zn / Å$^2$ | $\begin{pmatrix} 0.0095 \\ 0.0095 \\ 0.0095 \end{pmatrix}$ | $\begin{pmatrix} 0.036 \\ 0.036 \\ 0.036 \end{pmatrix}$ |
| Mean square displacement of Zn perpendicular to the Zn···Zn axis, $U_{\perp}$ / Å$^2$ | 0.0095 | 0.036 |
| Mean square displacement of Zn parallel to the Zn···Zn axis , $U_{\parallel}$ / Å$^2$ | 0.0095 | 0.036 |
| Mean displacement of Zn perpendicular to the Zn···Zn axis, $u_{\perp}$ / Å | 0.0975 | 0.190 |
| Mean displacement of C/N parallel to the Zn···Zn axis , $u_{\parallel}$ / Å | 0.0975 | 0.190 |

## 7. Calculation of the Lower and Upper Limits on Bond Lengths Derived from the Results of Rietveld Analysis of Neutron Diffraction Data

Using the treatment of Busing and Levy,[38] it is possible to place limits on the mean instantaneous bond length, $r_{p-q}$, between two atoms $p$ and $q$ using information obtained from the Rietveld analysis of the Bragg diffraction data (Table 3). Note, the symbols used in the original work by Busing and Levy have been changed in the equations presented below to be consistent with those used elsewhere in this work. Busing and Levy[38] showed that the mean instantaneous bond length, $r_{p-q}$, lies between two limits as follows

$$r^0_{p-q} + {U^2_L}/{2r^0_{p-q}} \leq r_{p-q} \leq r^0_{p-q} + {U^2_U}/{2r^0_{p-q}}$$

(Equation S.1)

where $U^2_L \; and \; U^2_U$ are defined as follows:

$$U^2_L \equiv \left[\left(U_{p\perp}\right)^{\frac{1}{2}} - \left(U_{q\perp}\right)^{\frac{1}{2}}\right]^2 \leq U^2 \leq \left[\left(U_{p\perp}\right)^{\frac{1}{2}} + \left(U_{q\perp}\right)^{\frac{1}{2}}\right]^2 \equiv U^2_U \quad \text{(Equation S.2)}$$

$U_{p\perp}$ and $U_{q\perp}$ are the relative vector displacement of the atoms $p$ and $q$ in the plane normal to the line between the mean atomic positions. These values are obtained as eigenvalues of the anisotropic displacement parameters (Table S.12). The lower and upper limits for the mean instantaneous bond length between two atoms $p$ and $q$, $r_{p-q}$, correspond to parallel (↑↑) and antiparallel (↑↓) motions of the two atoms, respectively.

## 8. X-ray Diffraction Measurement on $Zn(CN)_2$

A sample of $Zn(CN)_2$ was loaded into a silica glass capillary of internal diameter 1.0 mm and X-ray diffraction measurements were made at 295 K with a Panalytical X'Pert Pro Multipurpose Diffractometer, running in capillary mode, with a silver anode source ($\lambda$ = 0.560885 Å). Data were recorded using scattering angles, $2\theta$, from 3.2° to 156.0°, with a step of 0.2°, and the diffractometer was set up to optimise the count rate

(not the resolution). The diffraction pattern of the sample was measured for 98 hours, and an empty capillary and the empty instrument were measured for suitable durations to yield data with similar statistical accuracy to the data for the sample. The program GudrunX[34,39] was used to correct the data for multiple scattering, attenuation, polarisation, Compton scattering, Bremsstrahlung and fluorescence, and to achieve an absolute normalization (using the Krogh-Moe/Norman method[40,41]). The maximum useful momentum transfer, $Q_{max}$, was 19.5 Å$^{-1}$. The data were sharpened[42] using the square of the mean form factor, $\langle F\langle Q\rangle\rangle^2$, (rather than the mean square form factor,[43] $\langle F^2(Q)\rangle$) because for samples with elements of very different atomic number this leads to a correlation function peak shape which is narrower and has smaller wings. The total X-ray correlation function (Figures 7 and 8), $T^X(r)$, was then obtained by Fourier transformation of the interference function, $Qi^X(Q)$, using the Lorch modification function.[44]

## 9. Total Diffraction (Neutron and X-ray) Analysis of $Zn(CN)_2$

For total neutron diffraction analysis, the corrected and normalized data from four detector banks[30] (banks 2, 3, 4, 5 at average scattering angles of 17.3, 34.3, 61.7 and 91.8 °) were merged to yield an interference function, $Qi^N(Q)$, which covered the $Q$-range 1.0 - 51.5 Å$^{-1}$, and this was then extrapolated to $Q$ = 0 Å$^{-1}$ (Figure S.8). The total neutron correlation function (Figures 7 and 8), $T^N(r)$, was then obtained by Fourier transformation of the interference function, using the Lorch modification function.[44] The final normalization of the total diffraction results was achieved so that the low $r$ region of $T^N(r)$ is consistent with the average density contribution. Figure S.9 shows the differential neutron and X-ray correlation functions, $D(r)$, over a relatively wide range of $r$, from which the long-range order of the crystal is apparent. Table S.13 gives the parameters from fitting of the neutron correlation function, $T^N(r)$, at 11.4 and 295 K. Table S.14 gives the parameters from fitting of the X-ray correlation function, $T^X(r)$, at 295 K.

**Table S.13.** Structural Parameters (Interatomic Distance, $r_{p-q}$, RMS Variation in Interatomic Distance, $\left\langle u^2_{p-q} \right\rangle^{½}$, and Coordination Number, $n_{p-q}$[45]) for $Zn(CN)_2$ Obtained from Fitting the Neutron Correlation Functions, $T^N(r)$, at 11.4 and 295 K.

| Temperature / K | Atom pair[§] | | $r_{p-q}$ / Å | $\left\langle u^2_{p-q} \right\rangle^{½}$ / Å | $n_{p-q}$ |
|---|---|---|---|---|---|
| 11.4 | C≡N | ($r_1$) | 1.1510(3) | 0.0277(5) | 0.941(5) |
| | Zn−C/N | ($r_2$) | 1.9914(5) | 0.0555(6) | 4.07(3) |
| | Zn···C/N | ($r_3$) | 3.150(2) | 0.055(1) | 4* |
| | (C/N)···(C/N) | ($r_4$) | 3.239(1) | 0.109(2) | 3* |
| 295 | C≡N | ($r_1$) | 1.1502(3) | 0.0294(5) | 0.966(5) |
| | Zn−C/N | ($r_2$) | 1.9955(6) | 0.0672(7) | 3.99(3) |
| | Zn···C/N | ($r_3$) | 3.144(3) | 0.070(2) | 4* |
| | (C/N)···(C/N) | ($r_4$) | 3.255(3) | 0.147(3) | 3* |

[§]Lines between a pair of atoms indicate bonds, whilst dots indicate a non-bonded distance. The labels ($r_n$) refer to correlations shown in Figure 6.

*Number fixed at the ideal crystallographic value.

**Table S.14**. Structural parameters (interatomic distance, $r_{p-q}$, RMS variation in interatomic distance, $\left\langle u^2_{p-q} \right\rangle^{½}$, and coordination number, $n_{p-q}$[45]) for $Zn(CN)_2$, obtained from fitting the X-ray correlation function, $T^X(r)$, at 295 K. (Statistical errors from the fits are indicated by the values in brackets).

| Atom pair[§] | | $r_{p-q}$ / Å | $\left\langle u^2_{p-q} \right\rangle^{½}$ / Å | $n_{p-q}$ |
|---|---|---|---|---|
| Zn−C/N | ($r_2$) | 1.990(2) | 0.072(3) | 3.76(5) |
| Zn···C/N | ($r_3$) | 3.144[†] | 0.070[†] | 3.01(4) |
| (C/N)···(C/N) | ($r_4$) | 3.255[†] | 0.147[†] | 2.26(3) |

[§]Lines between a pair of atoms indicate bonds, whilst dots indicate a non-bonded distance.

[†]Value fixed from fitting the 295 K $T^N(r)$ data.

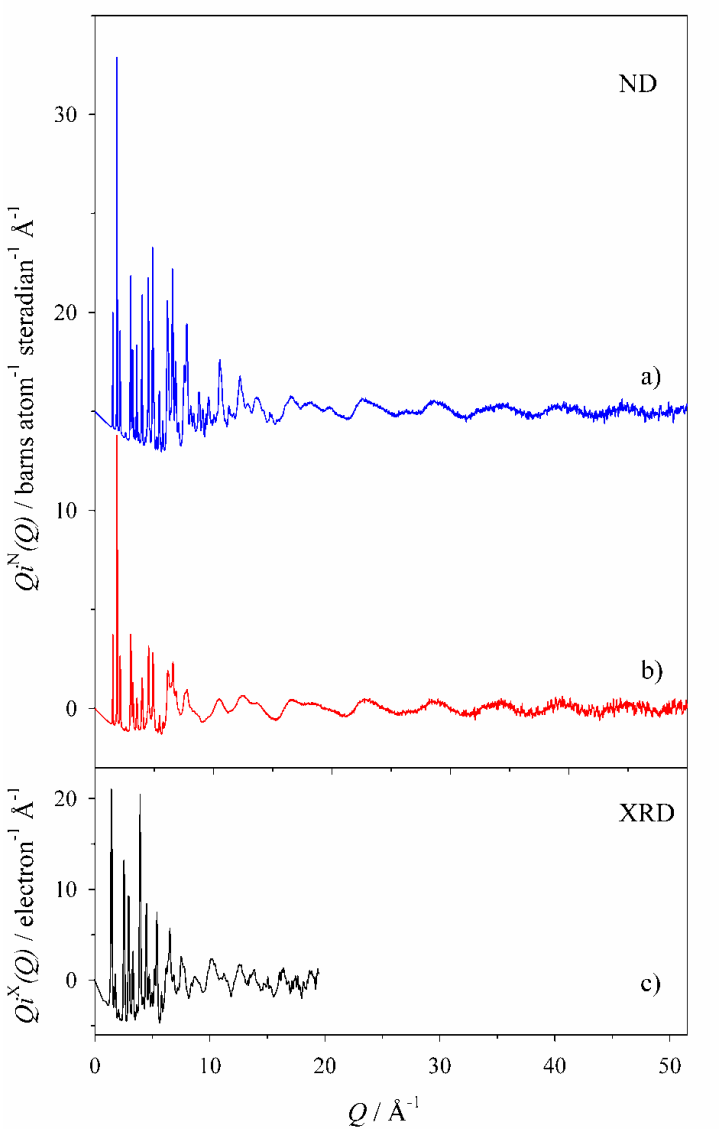


**Figure S.8.** The interference function, $Qi(Q)$, for $Zn(CN)_2$ measured by a) neutron diffraction at 11.4 K (vertically offset by 15 units), b) neutron diffraction at 295 K, and c) X-ray diffraction at 295 K.

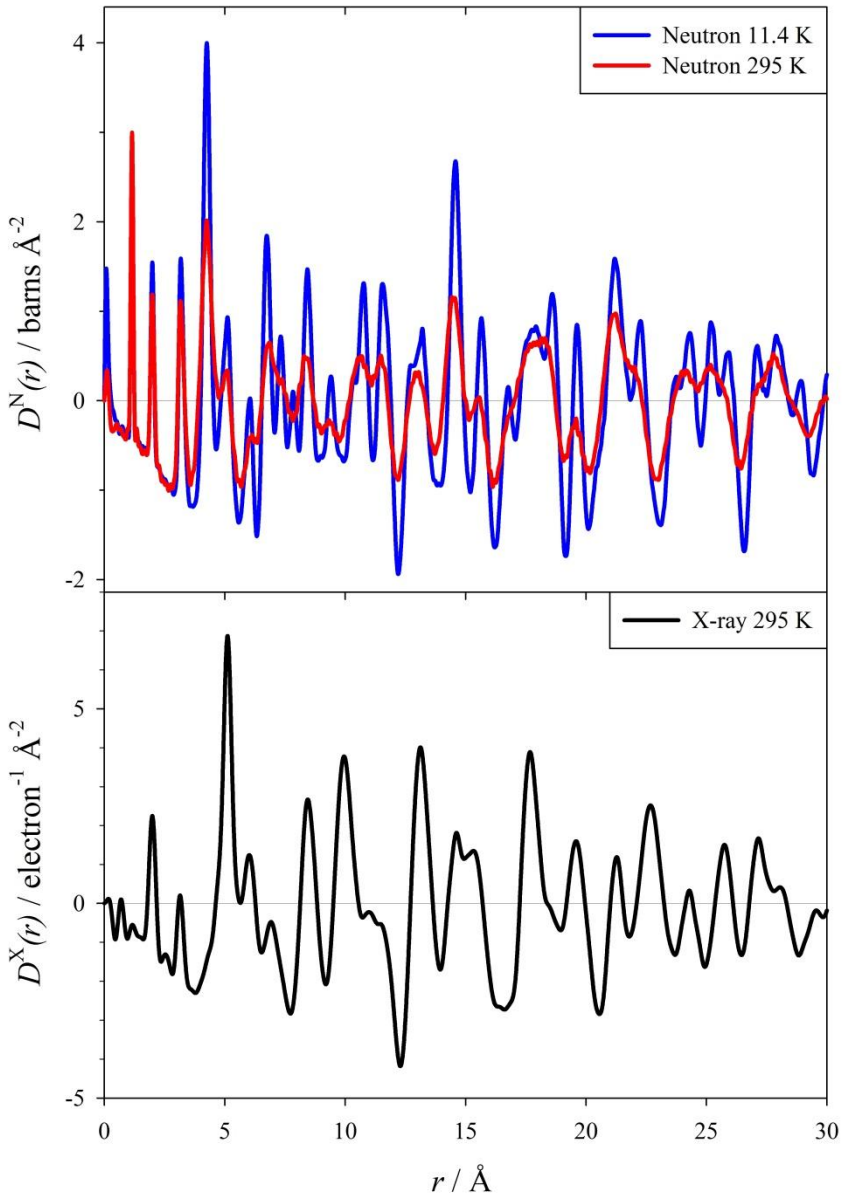


**Figure S.9.** The differential neutron correlation function, $D^N(r)$, of $Zn(CN)_2$ at 11.4 (top, blue) and 295 K (top, red), and the differential X-ray correlation function, $D^X(r)$, of $Zn(CN)_2$ at 295 K (bottom, black).

## 10. Fitting Procedure for $T^N(r)$ Incorporating Different Zn–C and Zn–N Bond Lengths

In order to investigate the possibility of a difference in Zn–C and Zn–N bond lengths, a computer program was written for fitting the neutron correlation function, $T^N(r)$, in the region from 1.0 to 3.55 Å. The aim of the fitting is to produce a set of interatomic distances which are physically consistent. Figure S.10 shows a Zn–C≡N–Zn linkage, which gives rise to six independent interatomic distances if there is a bond length difference. There is also a further contribution to $T^N(r)$ in the same distance range due to tetrahedral (C/N)···(C/N) distances. However, there are only three peaks in $T^N(r)$ in the relevant region, and only the third peak shows visible asymmetry. Thus it is not achievable to determine six different distances from a fitting procedure, and hence simplifying assumptions were made that the four atoms in a linkage are coplanar, and that the two atoms in a cyanide group are displaced the same distance, $\Delta$, from the Zn···Zn axis. For this model, all of the interatomic distances can be calculated from four independent parameters, which we chose to be $r_1$, $\Delta$, $r_{Zn\text{-}C}$ and $r_{Zn\cdots Zn}$. For a given set of these parameters, the lengths of the projections of the Zn–C and Zn–N bonds onto the Zn···Zn axis may be calculated as

$$p_C = \left(r_{Zn\text{-}C}^2 - \Delta^2\right)^{1/2} \qquad p_N = r_{Zn\cdots Zn} - r_1 - p_C \qquad \text{(Equation S.3)}$$

Then the dependent interatomic distances may be calculated as follows

$$r_{Zn\text{-}N}^2 = \Delta^2 + p_N^2$$

$$r_{Zn\cdots C}^2 = \left(r_{Zn\cdots Zn} - p_C\right)^2 + \Delta^2$$

$$r_{Zn\cdots N}^2 = \left(r_1 + p_C\right)^2 + \Delta^2 \qquad \text{(Equation S.4)}$$

where $r_{Zn\cdots C}$ and $r_{Zn\cdots N}$ are unbonded interatomic distances. The (C/N)···(C/N) contribution to the third peak in $T^N(r)$, arising from the edges of the $Zn(C/N)_4$ tetrahedra, was modeled using a single independent distance, $r_4$ (~3.24 Å). If the tetrahedra were all identical then the length of the edge of the tetrahedra would be dependent on the Zn–C or (Zn–N) bond length (i.e., $r_4=\sqrt{(8/3)}r_2$), but since five different $Zn(CN)_{4-n}(NC)_n$ tetrahedra are present, this is not appropriate, and hence $r_4$ was taken as an independent parameter.

In the fitting, the distance $r_{Zn\cdots Zn}$ was fixed at the value $a\sqrt{3}/2$, determined from Rietveld refinement, because the method of Busing and Levy[38] (Table 3) shows that this is a good measure of the average Zn···Zn separation. There are then four independent distances in the fitting, $r_1$, $\Delta$, $r_{Zn\text{-}C}$ and $r_4$, which is the maximum number which can reliably be extracted from two symmetric peaks and one asymmetric peak. In the fitting, the same value was used for the RMS variation in the Zn–C and Zn–N bond lengths; similarly, the same value was used for the RMS variation in the Zn···C and Zn···N distances. The coordination numbers corresponding to the various contributions to the peaks at distances $r_2$, $r_3$ and $r_4$ were all scaled by the same factor to take into account experimental error in coordination number.

The correlation function measured at 11.4 K was fitted first, and a successful fit could not be achieved unless $\Delta$ was fixed at zero; otherwise the fit diverged. A value of zero for $\Delta$ corresponds to a linear Zn–C≡N–Zn linkage, and this is reasonable because at low temperature only atomic vibrations with longer wavelength are significantly populated, in which case there is little deviation from linearity of an individual linkage. For a linear linkage, the equations relating the interatomic distances (Equations S.3 and S.4) simplify to

$$r_{Zn\cdots C}=r_{Zn\cdots Zn}-r_{Zn\text{-}C} \qquad r_{Zn\cdots N}=r_1+r_{Zn\text{-}C} \qquad \text{(Equation S.5)}$$

The results from the fit to $T^N(r)$ at 11.4 K (Figure S.11) are given in Table S.15, and the bond length difference determined in this way is reasonable, as discussed in the main text. A satisfactory fit to $T^N(r)$ at 295 K in which the bond length difference (i.e., the independent parameter $r_{Zn\text{-}C}$) could not be obtained, due to the greatly increased width of the peak at distance $r_4$ (Table 3). Consequently the fit to the 295 K data given in Table S.15 was performed with the Zn–C bond length fixed at the value obtained from the fit to the 11.4 K data; this is a reasonable constraint since there is strong evidence that bond lengths change very little with temperature.

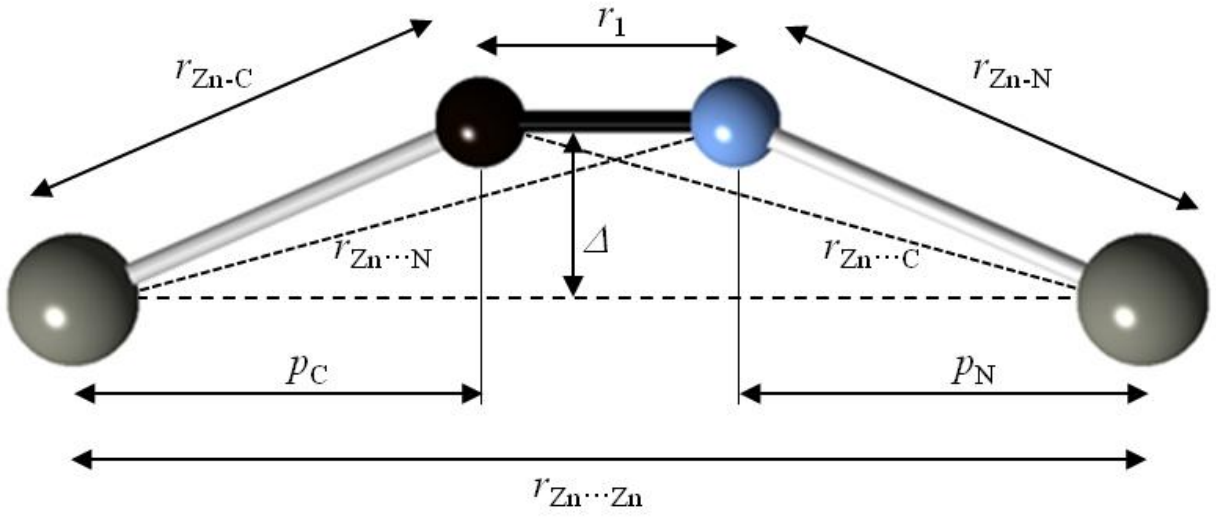


**Figure S.10.** Definition of distances used in bond length difference fits with Zn, C and N atoms shown as gray, black and blue spheres respectively. The atoms are coplanar and the C and N atoms are assumed to be displaced the same distance from the Zn···Zn axis.

**Table S.15**. Structural parameters (interatomic distance, $r_{i-j}$, RMS variation in interatomic distance, $\langle u_{i-j}^2 \rangle^{½}$, and coordination number, $n_{i-j}$[45]) for $Zn(CN)_2$, obtained from bond length difference fits to the neutron correlation function, $T^N(r)$, at 11.4 and 295 K. (Statistical errors from the fits are indicated by the values in brackets.)

| Temperature / K | Cyanide displacement, $\Delta$ / Å | Atom pair[§] | | $r_{i-j}$ / Å | $\langle u_{i-j}^2 \rangle^{½}$ / Å | $n_{i-j}$ |
|---|---|---|---|---|---|---|
| 11.4 | 0.0* | C≡N | ($r_1$) | 1.1512(3) | 0.0277(6) | 0.941(5) |
| | | Zn–N<br>Zn–C | ($r_2$) | 1.969(2) †<br>2.030(2) | 0.044(2) | 1.971(8) |
| | | Zn···C<br>Zn···N | ($r_3$) | 3.120(2) †<br>3.181(2) † | 0.045(2) | 1.971(8) † |
| | | (C/N)···(C/N) | ($r_4$) | 3.235(1) | 0.111(1) | 2.96(1) † |
| 295 | 0.266(4) | C≡N | ($r_1$) | 1.1501(3) | 0.0295(5) | 0.966(5) |
| | | Zn–N<br>Zn–C | ($r_2$) | 1.972 †<br>2.030* | 0.062(1) | 2.04(1) |
| | | Zn···C<br>Zn···N | ($r_3$) | 3.116 †<br>3.173 † | 0.068(1) | 2.04(1) † |
| | | (C/N)···(C/N) | ($r_4$) | 3.246(2) | 0.148(2) | 3.06(1) † |

[§]Lines between a pair of atoms indicate bonds, whilst dots indicate a non-bonded distance.
†dependent parameter; *value fixed during refinement.

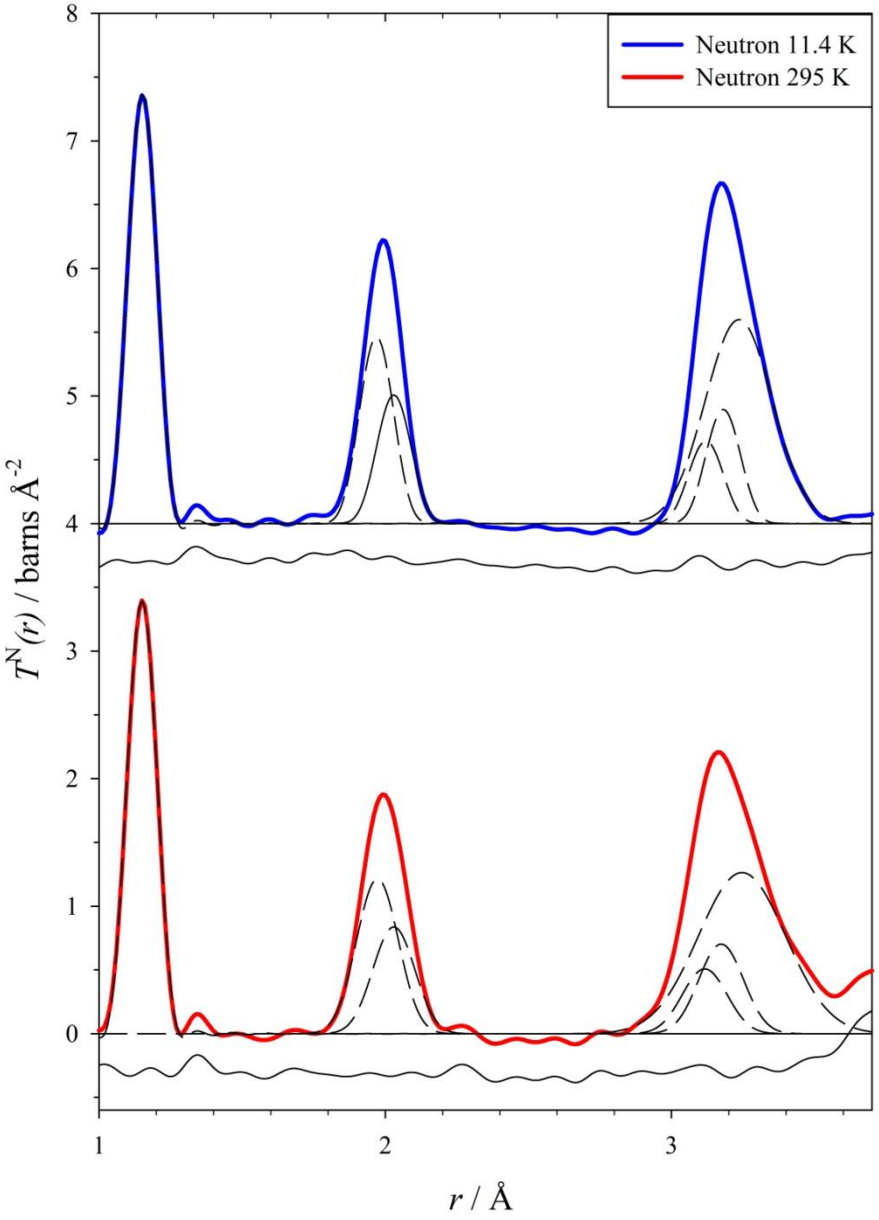


**Figure S.11.** Peak fits to $T^N(r)$ at 11.4 K (vertically offset) and 295 K, to determine the difference in Zn–N and Zn–C bond lengths. The individual components of the fit are shown by dashed lines, and the residual is shown by a displaced continuous line.

## 11. The Effect of Transverse Atomic Motion on the Zn–N and Zn–C Bond Lengths at 11.4 and 295 K

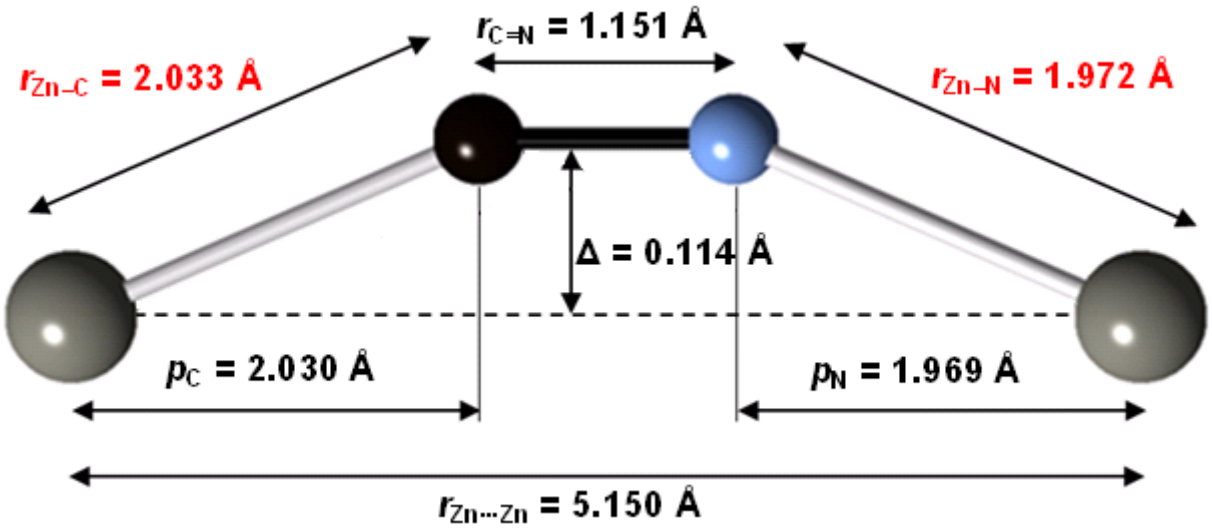


**Figure S.12.** *Skipping-rope* mode at 11.4 K. Zn, C and N atoms are shown as gray, black and blue spheres respectively. The atoms are coplanar and the C and N atoms are assumed to be displaced the same distance from the Zn···Zn axis.

It is assumed that Zn···Zn = 5.150 Å (from Rietveld refinement at 11.4 K, Table 3), C≡N bond length, $r_1$ = 1.151Å (from total neutron correlation function, Table 3), $\Delta = u_\perp =$ 0.114 Å (from Rietveld refinement, Table S.12), $p_N$ = 1.969 Å and $p_C$ = 2.030 Å (from total neutron correlation function, Table S.15).

**Therefore, from Pythagoras, $r_{Zn-N}$ = 1.972 Å and $r_{Zn-C}$ = 2.033 Å**

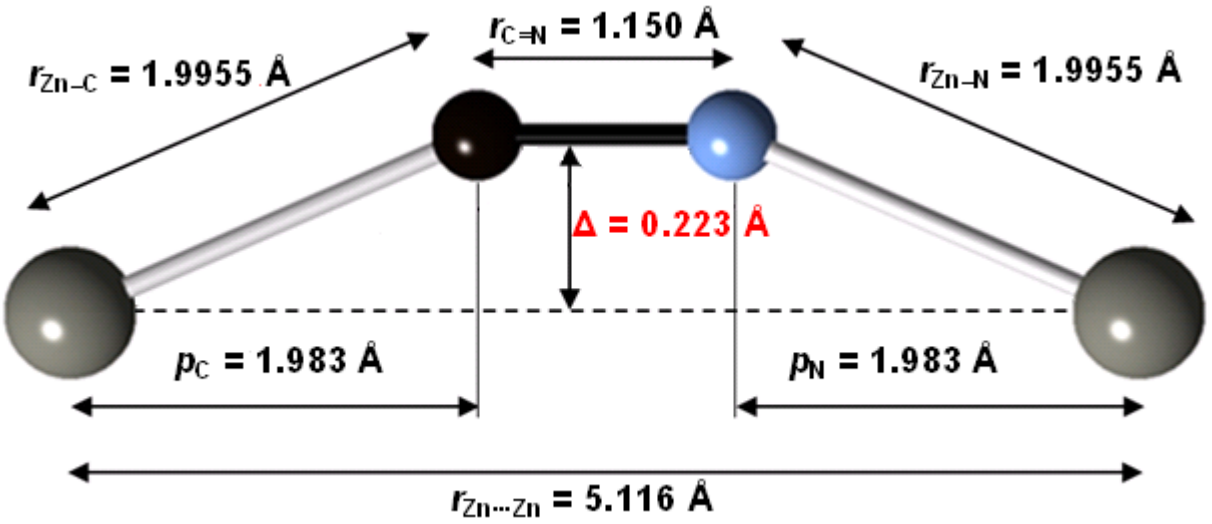


**Figure S.13.** *Skipping-rope* mode at 295 K. The atoms are coplanar and the C and N atoms are assumed to be displaced the same distance from the Zn···Zn axis. Key as for Figure S.12.

It is assumed that Zn···Zn = 5.116 Å (from Rietveld refinement at 295 K, Table 3), C≡N bond length, $r_1$ = 1.150Å (from total neutron correlation function, Table 3), $r_{Zn-N}$ = $r_{Zn-C}$ = 1.9955Å (from total neutron correlation function, Table 3). Hence, $p_N$ = $p_C$ = 1.983 Å.

**Therefore, from Pythagoras Δ = 0.223 Å**

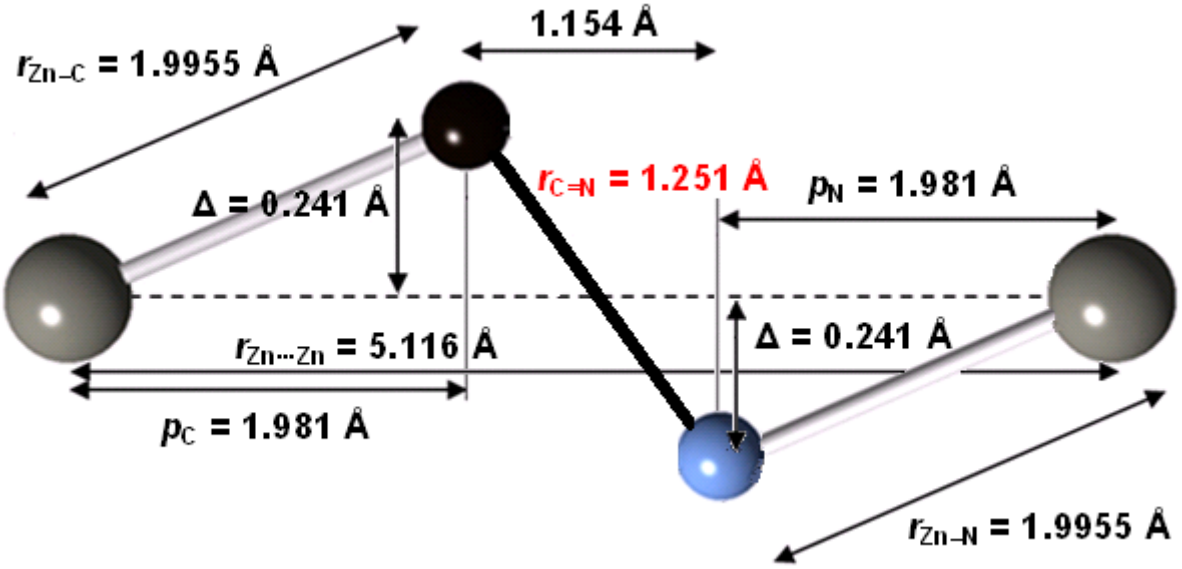


**Figure S.14.** *Kinky* mode at 295 K. The atoms are coplanar and the C and N atoms are assumed to be displaced the same distance from the Zn···Zn axis. Key as for Figure S.12.

It is assumed that Zn···Zn = 5.116 Å (from Rietveld refinement at 295 K, Table 3), $\Delta = u_{\perp} =$ 0.241 Å (from Rietveld refinement, Table S.12), $r_{Zn-N} = r_{Zn-C}$ = 1.9955Å (from total neutron correlation function, Table 3). Hence, $p_N = p_C$ = 1.981 Å.

**Therefore, from Pythagoras, C ≡N bond length, $r_1$ = 1.251Å i.e., unfeasibly long**

## 12. Bond Lengths in $Zn(CN)_4$ and $Zn(NC)_4$ Tetrahedra in Crystalline Metal Cyanides

In mixed-metal cyanides with M−C≡N−M' linkages in which one of the metals is zinc, the C≡N groups are ordered with zinc bonded to the nitrogen end of the cyanide ligand (Table S.16). The crystal structures listed in Table S.16 give an average Zn–N bond length of 1.966(12) Å in $Zn(N{\equiv}C{-}M'{-})_4$ coordination. Bonds from zinc to the carbon end of the cyanide ligand are only found in $Zn(CN)_2$ and in compounds containing isolated tetrahedral $[Zn(CN)_4]^{2-}$ complex anions. Four such crystal structures have been reported in which Zn is bonded to carbon in Zn–C≡N links.[46-49] Of these, only one, $K_2Zn(CN)_4$,[50] is a well-determined structure at atmospheric pressure (i.e., with C≡N bond lengths close to the accepted value of 1.15 Å). In $K_2Zn(CN)_4$, the C≡N and Zn–C bond lengths are 1.155(9) and 2.018(7) Å, respectively.

**Table S.16.** The C≡N and Zn–N bond lengths in crystalline mixed-metal cyanides in which zinc is in tetrahedral coordination and bonded to the nitrogen end of the cyanide ligand.

| | C≡N bond lengths / Å | Mean Zn–N bond length / Å |
|---|---|---|
| $(N(CH_3)_4)Zn(Cu(CN)_4)$ (low-temperature phase) [51] | 1.134, 1.155 | 1.956 |
| $Zn_3(Co(CN)_6)_2$ [52] | 1.148, 1.154 | 1.969 |
| $Zn_3(Fe(CN)_6)_2$ [52] | 1.154, 1.161 | 1.984 |
| $Rb_2Zn_3(Fe(CN)_6)_2.xH_2O$ [52] | 1.141, 1.144 | 1.980 |
| $(NH_4)_2Zn_3(Fe(CN)_6)_2.xH_2O$ [52] | 1.146, 1.150 | 1.965 |
| $(H_3O)_2Zn_3(Re_6Se_8(CN)_6)_2{\cdot}20H_2O$ [53] | 1.149, 1.163 | 1.964 |
| $Cs_2Zn_3(Fe(CN)_6)_2(H_2O)_6$ [54] | 1.146, 1.148 | 1.964 |
| $K_2Zn_3(Fe(CN)_6)_2.xH_2O$ [55] | 1.153 | 1.948 |
| Average: | 1.150(7) | 1.966(12) |

Difference between the mean bond lengths, Zn–C and Zn–N, is 2.018(7) – 1.966(12) = 0.052 Å.

## 14. Infrared and Raman Spectra of $Zn(CN)_2$

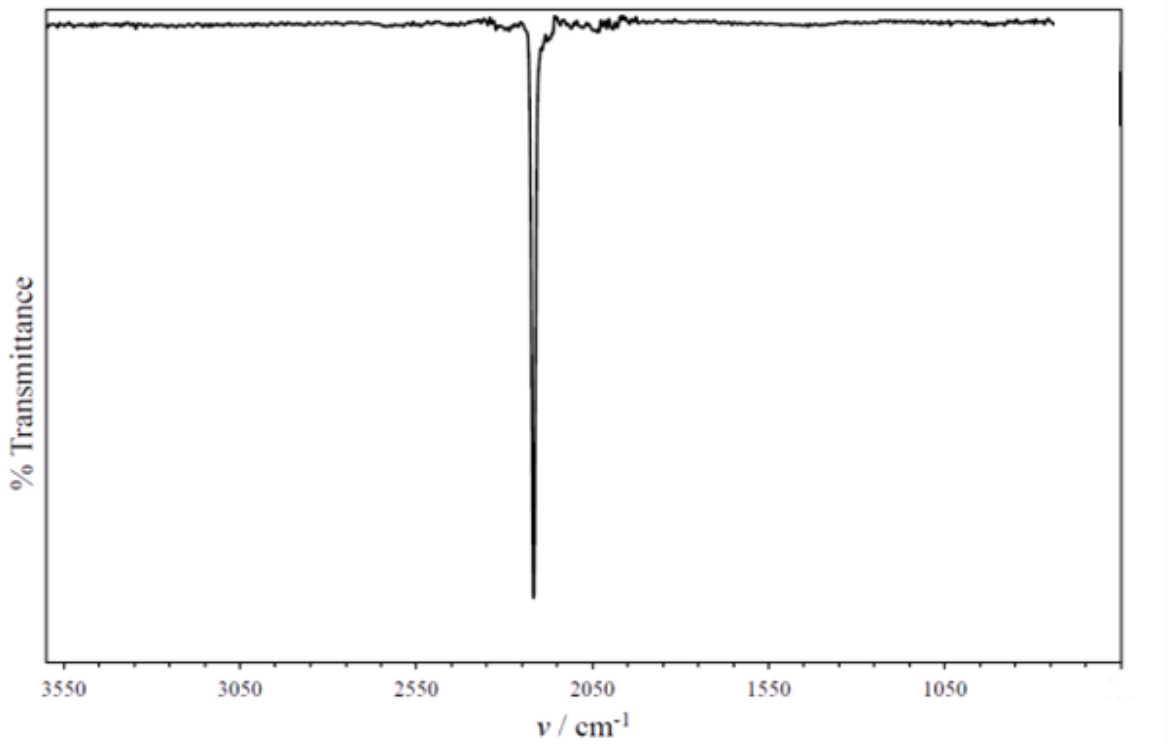


**Figure S.15.** IR spectrum of $Zn(CN)_2$ (range 3550 – 750 $cm^{-1}$). $\bar{\nu}_{C\equiv N}$ occurs at 2216 $cm^{-1}$.

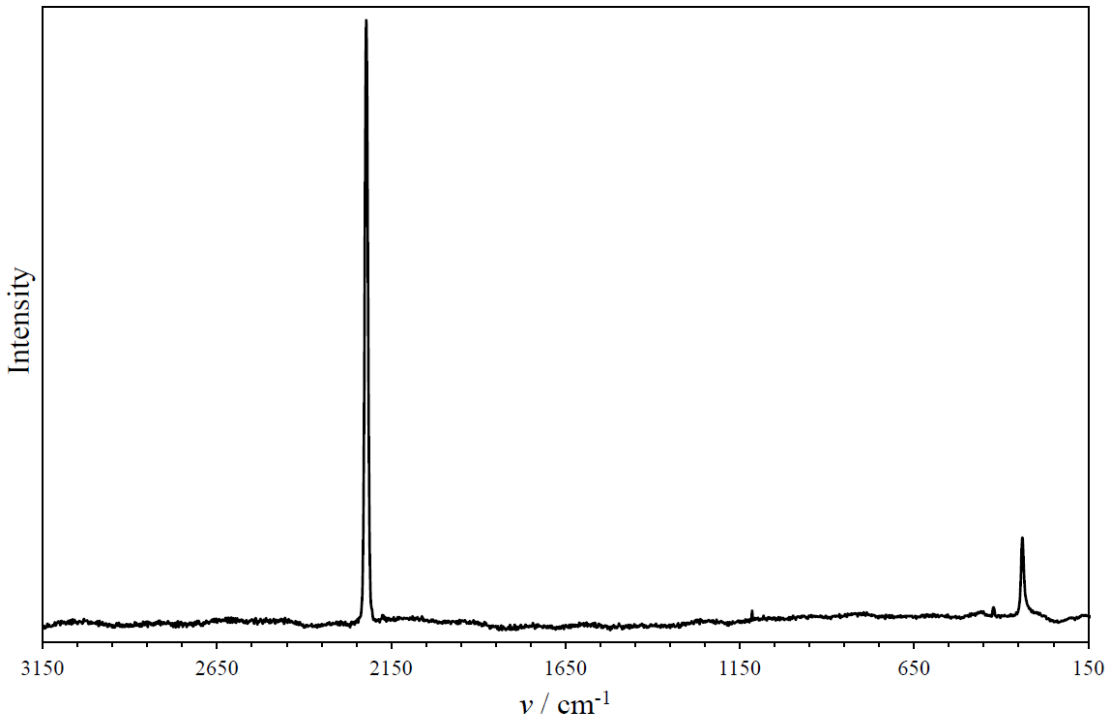


**Figure S.16.** Raman spectrum of $Zn(CN)_2$. $\bar{\nu}_{C\equiv N}$ and $\bar{\nu}_{Zn\text{-}C/N}$ occur at 2216 and 335 $cm^{-1}$ respectively.

**References**


(1) Sutrisno, A.; Liu, L.; Xu, J.; Huang, Y. N. *Phys. Chem. Chem. Phys.* **2011**, *13*, 16606.

(2) Frisch, M. J.; Trucks, G. W.; Schlegel, H. B.; Scuseria, G. E.; Robb, M. A.; Cheeseman, J. R.; Montgomery, J., J.A.; Vreven, T.; Kudin, K. N.; Burant, J. C.; Millam, J. M.; Iyengar, S. S.; Tomasi, J.; Barone, V.; Mennucci, B.; Cossi, M.; Scalmani, G.; Rega, N.; Petersson, G. A.; Nakatsuji, H.; Hada, M.; Ehara, M.; Toyota, K.; Fukuda, R.; Hasegawa, J.; Ishida, M.; Nakajima, T.; Honda, Y.; Kitao, O.; Nakai, H.; Klene, M.; Li, X.; Knox, J.; Hratchian, H. P.; Cross, J. B.; Bakken, V.; Adamo, C.; Jaramillo, J.; Gomperts, R.; Stratmann, R. E.; Yazyev, O.; Austin, A. J.; Cammi, R.; Pomelli, C.; Ochterski, J. W.; Ayala, P. Y.; Morokuma, K.; Voth, G. A.; Salvador, P.; Dannenberg, J. J.; Zakrzewski, V. G.; Dapprich, S.; Daniels, A. D.; Strain, M. C.; Farkas, O.; Malick, D. K.; Rabuck, A. D.; Raghavachari, K.; Foresman, J. B.; Ortiz, J. V.; Cui, Q.; Baboul, A. G.; Clifford, S.; Cioslowski, J.; Stefanov, B. B.; Liu, G.; Liashenko, A.; Piskorz, P.; Komaromi, I.; Martin, R. K.; Fox, D. J.; Keith, T.; Al-Laham, M. A.; Peng, C. Y.; Nanayakkara, A.; Challacombe, M.; Gill, P. M. W.; Johnson, B.; Chen, W.; Wong, M. W.; Conzalez, C.; Pople, J. A., Gaussian 03, **2003**, version G03.

(3) Becke, A. D. *J. Chem. Phys.* **1993**, *98*, 5648.

(4) Lee, C.; Yang, W.; Parr, R. G. *Phys. Rev. B* **1988**, *37*, 785.

(5) Stephens, P. J.; Devlin, F. J.; Chablowski, C. F.; Frisch, M. J. *J. Phys. Chem.* **1994**, *98*, 11623.

(6) Vosko, S. H.; Wilk, L.; Nusaur, M. *Can. J. Phys.* **1980**, *58*, 1200.

(7) Raghavachari, K.; Trucks, G. W. *J. Chem. Phys.* **1989**, *91*, 1062.

(8) McLean, A. D.; Chandler, G. S. *J. Chem. Phys.* **1980**, *72*, 5639.

(9) Raghavachari, K.; Binkley, J. S.; Seeger, R.; Pople, J. A. *J. Chem. Phys.* **1980**, *72*, 4244.

(10) Kendall, R. A.; Dunning, T. H.; Harrison, R. J. *J. Chem. Phys.* **1992**, *96*, 6796.

(11) Woon, D. E.; Dunning, T. H. *J. Chem. Phys.* **1993**, *98*, 1358.

(12) Segall, M. D.; Lindan, P. J. D.; Probert, M. J.; Pickard, C. J.; Hasnip, P. J.; Clark, S. J.; Payne, M. C. *J. Phys.: Condens. Matter* **2002**, *14*, 2717.

(13) Perdew, J. P.; Burke, K.; Ernzerhof, M. *Phys. Rev. Lett.* **1996**, *77*, 3865.

(14) Perdew, J. P.; Burke, K.; Ernzerhof, M. *Phys. Rev. Lett.* **1998**, *80*, 891.

(15) Profeta, M.; Mauri, F.; Pickard, C. J. *J. Am. Chem. Soc.* **2003**, *125*, 541.

(16) Pickard, C. J.; Mauri, F. *Phys. Rev. B* **2001**, *63*, 245101.

(17) Yates, J. R.; Pickard, C. J.; Mauri, F. *Phys. Rev. B* **2007**, *76*, 024401.

(18) Bak, M.; Rasmussen, J. T.; Nielsen, N. C. *J. Magn. Reson.* **2000**, *147*, 296.

(19) Harris, R. K.; Olivieri, A. C. *Prog. Nucl. Mag. Res. Sp.* **1992**, *24*, 435.

(20) Kroeker, S.; Wasylishen, R. E.; Hanna, J. V. *J. Am. Chem. Soc.* **1999**, *121*, 1582.

(21) Wu, G.; Kroeker, S.; Wasylishen, R. E. *Inorg. Chem.* **1995**, *34*, 1595.

(22) Kroeker, S.; Wasylishen, R. E. *Canadian Journal of Chemistry-Revue Canadienne De Chimie* **1999**, *77*, 1962.

(23) Chapman, K. W.; Chupas, P. J.; Kepert, C. J. *J. Am. Chem. Soc.* **2005**, *127*, 15630.

(24) Goodwin, A. L.; Kepert, C. J. *Phys. Rev. B* **2005**, *71*, 140301R.

(25) Zhdanov, G. S. *Dokl. Akad. Nauk SSSR* **1941**, *31*, 352.

(26) Hoskins, B. F.; Robson, R. *J. Am. Chem. Soc.* **1990**, *112*, 1546.

(27) Kitazawa, T.; Nishikiori, S. I.; Kuroda, R.; Iwamoto, T. *J. Chem. Soc. Dalton* **1994**, *1994*, 1029.

(28) Williams, D. J.; Partin, D. E.; Lincoln, F. J.; Kouvetakis, J.; O'Keeffe, M. *J. Solid State Chem.* **1997**, *134*, 164.

(29) Reckeweg, O.; Simon, A. *Z Naturforsch B* **2002**, *57*, 895.

(30) Hannon, A. C. *Nucl. Instrum. Meth. A* **2005**, *551*, 88.

(31) Hannon, A. C. In *Encyclopedia of Spectroscopy and Spectrometry*; Lindon, J., Tranter, G., Holmes, J., Eds.; Academic Press: London, 2000; Vol. 2; pp 1479.

(32) Nakatsuka, A.; Yoshiasa, A.; Yamanaka, T. *Acta Cryst. B* **1999**, *55*, 266.

(33) Ikeda, S.; Carpenter, J. M. *Nucl. Instrum. Meth. A* **1985**, *239*, 536.

(34) Soper, A. K. Rutherford Appleton Laboratory Technical Report, RAL-TR-2011-013, 2011.

(35) Hannon, A. C.; Howells, W. S.; Soper, A. K. *Inst. Phys. Conf. Ser.* **1990**, *107*, 193.

(36) Larson, A. C.; Von Dreele, R. B. Los Alamos Report, LAUR 86-748, 2004.

(37) Toby, B. H. *J. Appl. Cryst.* **2001**, *34*, 210.

(38) Busing, W. R.; Levy, H. A. *Acta Cryst.* **1964**, *17*, 142.

(39) Soper, A. K.; Barney, E. R. *J. Appl. Cryst.* **2011**, *44*, 714.

(40) Krogh-Moe, J. *Acta Cryst.* **1956**, *9*, 951.

(41) Norman, N. *Acta Cryst.* **1957**, *10*, 370.

(42) Finbak, C. *Acta Chem. Scand.* **1949**, *3*, 1279.

(43) Soper, A. K. *J. Phys.: Condens. Matter* **2007**, *19*, 335206.

(44) Lorch, E. *J. Phys. C* **1969**, *2*, 229.

(45) Hannon, A. C.; Grimley, D. I.; Hulme, R. A.; Wright, A. C.; Sinclair, R. N. *J. Non-Cryst. Solids* **1994**, *177*, 299.

(46) Wiehl, L.; Kluefers, P.; Schweiss, B. P.; Fuess, H. *Z. Kristallogr.* **1988**, *184*, 281.

(47) Ahsbahs, H. *Z. Kristallogr.* **1981**, *154*, 243.

(48) Ahsbahs, H. *Z. Kristallogr.* **1979**, *149*, 151.

(49) Sequeira, A.; Chidambaram, R. *Acta Cryst.* **1966**, *20*, 910.

(50) Hoskins, B. F.; Robson, R.; Scarlett, N. V. Y. *Angew. Chem. Int. Edit.* **1995**, *34*, 1203.

(51) Phillips, A. E.; Halder, G. J.; Chapman, K. W.; Goodwin, A. L.; Kepert, C. J. *J. Am. Chem. Soc.* **2010**, *132*, 10.

(52) Rodriguez Hernandez, J.; Reguera, E.; Lima, E.; Balmaseda, J.; Martinez-Garcia, R.; Yee-Madeira, H. *J. Phys. Chem. Solids* **2007**, *68*, 1630.

(53) Naumov, N. G.; Virovets, A. V.; Fedorov, V. E. *Inorg. Chem. Commun.* **2000**, *3*, 71.

(54) Gravereau, P.; Garnier, E. *Rev. Chim. Miner.* **1983**, *20*, 68.

(55) Gravereau, P.; Garnier, E.; Hardy, A. M. *Acta Cryst. B* **1979**, *35*, 2843.